Improved aerosol processes and effective radiative forcing in HadGEM3 and UKESM1

Journal of Advances in Modeling Earth Systems

RESEARCH ARTICLE
10.1029/2018MS001464

Special Section:
The UK Earth System Models for CMIP6

Improved Aerosol Processes and Effective Radiative Forcing in HadGEM3 and UKESM1

J. P. Mulcahy[1], C. Jones[2], A. Sellar[1], B. Johnson[1], I. A. Boutle[1], A. Jones[1], T. Andrews[1], S. T. Rumbold[3], J. Mollard[4], N. Bellouin[4], C. E. Johnson[1], K. D. Williams[1], D. P. Grosvenor[2], and D. T. McCoy[5]

[1]Met Office, Exeter, UK, [2]National Centre for Atmospheric Science, University of Leeds, Leeds, UK, [3]National Centre for Atmospheric Science, University of Reading, Reading, UK, [4]Department of Meteorology, University of Reading, Reading, UK, [5]Institute of Climate and Atmospheric Sciences, University of Leeds, Leeds, UK

Abstract Aerosol processes and, in particular, aerosol-cloud interactions cut across the traditional physical-Earth system boundary of coupled Earth system models and remain one of the key uncertainties in estimating anthropogenic radiative forcing of climate. Here we calculate the historical aerosol effective radiative forcing (ERF) in the HadGEM3-GA7 climate model in order to assess the suitability of this model for inclusion in the UK Earth system model, UKESM1. The aerosol ERF, calculated for the year 2000 relative to 1850, is large and negative in the standard GA7 model leading to an unrealistic negative total anthropogenic forcing over the twentieth century. We show how underlying assumptions and missing processes in both the physical model and aerosol parameterizations lead to this large aerosol ERF. A number of model improvements are investigated to assess their impact on the aerosol ERF. These include an improved representation of cloud droplet spectral dispersion, updates to the aerosol activation scheme, and black carbon optical properties. One of the largest contributors to the aerosol forcing uncertainty is insufficient knowledge of the preindustrial aerosol climate. We evaluate the contribution of uncertainties in the natural marine emissions of dimethyl sulfide and organic aerosol to the ERF. The combination of model improvements derived from these studies weakens the aerosol ERF by up to 50% of the original value and leads to a total anthropogenic historical forcing more in line with assessed values.

Key Points:
- The HadGEM3-GA7 climate model has a large, negative aerosol ERF resulting in an unrealistic negative total anthropogenic forcing of climate
- The aerosol ERF is shown to be highly sensitive to the underlying physical and aerosol model processes and parameterizations
- Through a combination of scientific model improvements the aerosol ERF is reduced by up to 50% from −2.75 to −1.45 W/m^2

Correspondence to:
J. P. Mulcahy,
jane.mulcahy@metoffice.gov.uk

Citation:
Mulcahy, J. P., Jones, C., Sellar, A., Johnson, B., Boutle, I. A., Jones, A., et al. (2018). Improved aerosol processes and effective radiative forcing in HadGEM3 and UKESM1. *Journal of Advances in Modeling Earth Systems*, *10*, 2786–2805. https://doi.org/10.1029/2018MS001464

Received 3 AUG 2018
Accepted 10 OCT 2018
Accepted article online 15 OCT 2018
Published online 10 NOV 2018

1. Introduction

The UK Earth System Model version 1 (UKESM1) is the latest state-of-the-art UK Earth system model. UKESM1 builds on the latest HadGEM3 Global Coupled (GC) climate configuration of the Met Office Unified Model, which describes the core physical-dynamical processes of the land, atmosphere (Walters et al., 2017), ocean (Storkey et al., 2018), and sea ice systems (Ridley et al., 2018). UKESM1 extends this physical-dynamical model to also include key marine and terrestrial biogeochemical cycles, such as carbon and nitrogen cycles, fully interactive stratospheric-tropospheric trace gas chemistry, and an interactive continental ice sheet model. Feedbacks between these components are incorporated where they provide an important (amplifying or damping) feedback onto physical climate change and/or change themselves in response to changes in the physical climate and thereby impact society or natural ecosystems. Atmospheric aerosols are one important component of this model due to their direct impact on the radiation characteristics of the atmosphere (termed aerosol-radiation interactions, ARIs) and by indirectly modifying cloud and precipitation processes (termed aerosol-cloud interactions, ACIs). Aerosols also interact with atmospheric chemistry and biogeochemical cycles in the atmosphere, ocean, and ice surfaces (Carslaw et al., 2010; Kok et al., 2018; Scott et al., 2018; Quinn & Bates, 2011). Yet the influence of anthropogenic aerosol emissions on climate, in particular, cloud properties, remains one of the largest uncertainties in anthropogenic climate forcing estimates (Myhre, Shindell, et al., 2013).

The perturbation to climate by different forcing agents in global climate models (GCMs) is increasingly quantified by the effective radiative forcing (ERF; Andrews, 2014; Andrews et al., 2017; Paynter & Frölicher, 2015; Shindell et al., 2013). In contrast to the traditional radiative forcing metric the ERF incorporates fast perturbation responses, such as changes in cloud cover, and is therefore a better representation of the historical global mean temperature change (Forster et al., 2016; Sherwood et al., 2015). The aerosol ERF quantifies the climate

response to a positive perturbation in anthropogenic aerosol emissions since the preindustrial (PI) era. It is one of the largest contributors to the total anthropogenic ERF (Myhre, Shindell, et al., 2013) and shows a strong correlation with simulated changes in global mean surface temperature over the historical period (Rotstayn et al., 2015). However, estimates of the aerosol ERF remain highly uncertain (Boucher et al., 2013), and this has led to much debate on what defines a *credible* aerosol ERF range (Kretzschmar et al., 2017; Stevens, 2015).

The degree of uncertainty in the aerosol ERF is dependent on uncertainties not only in the aerosol processes themselves but also in the underlying physical model processes (Regayre et al., 2018; Zelinka et al., 2014). There is large diversity in global aerosol distributions, mixing state, lifetimes, and optical properties in GCMs (Kinne et al., 2006; Mann et al., 2014; Textor et al., 2006). Natural aerosol emissions, an important determinant of the PI aerosol climate used in aerosol ERF calculations, also remain highly unconstrained (Carslaw et al., 2013). Compounding these uncertainties is a lack of detailed understanding of the complex nature of aerosol-cloud-radiation interactions and the physical processes underpinning these interactions from both an observational and modeling perspective (Ghan et al., 2016; Lohmann & Feichter, 2005; Quaas et al., 2009; Seinfeld et al., 2016). This leads to various, often simplified treatments of these interactions in GCMs, which adds to the diversity in aerosol ERF estimates (Nazarenko et al., 2017; Wilcox et al., 2015). For instance, the aerosol-cloud forcing depends on the realism of the cloud macrophysical and microphysical processes in individual models and few GCMs include ACIs in ice phase clouds or parameterized convective clouds.

Simulations from the HadGEM3 physical model and UKESM1 models will constitute the bulk of the UK's contribution to the next Coupled Model Intercomparison Project phase 6 (CMIP6; Eyring et al., 2016). As part of the development of these two models the historical ERF of the main climate forcing agents is assessed, including well-mixed greenhouse gases, aerosols, tropospheric ozone, and land use. For UKESM1, the acceptance criterion requires the total (all forcing agents) historical anthropogenic ERF to be greater than 0 W/m^2. The Intergovernmental Panel on Climate Change 5th Assessment Report (IPCC AR5) report with *certainty* that the total anthropogenic ERF is positive (Myhre, Shindell, et al., 2013) and that the global climate has warmed since PI times (Hartmann et al., 2013).

In this paper, we focus on the assessment of the aerosol ERF, calculated for the year 2000 relative to 1850, in the atmosphere component of HadGEM3-GC3, termed the Global Atmosphere 7 configuration (GA7), as part of establishing the suitability of this model for inclusion in UKESM1. Section 2 diagnoses the aerosol ERF in the GA7 model and discusses the implications for passing the UKESM1 acceptance criterion. We subsequently investigate processes that are missing or poorly represented in the model that may have a significant impact on the aerosol ERF. By implementing or improving such processes we examine their impacts on the aerosol ERF in section 3. Section 5 evaluates the impact of these model changes on the present-day (PD) climate where we apply the additional criterion that they do not degrade the good performance of GA7 as described in Walters et al. (2017). Our overall aim is to develop an improved physical and Earth system model built solidly on GA7 that is suitable for use in CMIP6.

2. Diagnosing Aerosol ERF in GA7

As already stated above we use the HadGEM3-GA7 (hereafter referred to as GA7) climate model configuration (Walters et al., 2017) to calculate the historical ERF due to a PD aerosol perturbation. In this model global aerosol distributions and properties are simulated using the Global Model of Aerosol Processes (GLOMAP-Mode; Mann et al., 2010). GLOMAP-Mode is a double-moment aerosol microphysics model, simulating the mass and number of sulfate, sea salt, organic carbon (OC), and black carbon (BC) aerosol species across five log-normal size modes. Mineral dust is simulated separately using the Woodward (2001) bin emission scheme. Simulated aerosol particles modify radiation fluxes through the direct scattering and absorption of shortwave (SW) and longwave (LW) radiation as outlined in Bellouin et al. (2013). Aerosol particles can alter liquid cloud properties when they are activated into cloud droplets. The number of activated cloud droplets, N_d, is simulated using the UKCA-Activate scheme (West et al., 2014). This aerosol activation scheme is based on the parameterization of Abdul-Razzak and Ghan (2000), which uses a combination of Köhler theory and empirical fits to detailed cloud parcel models to calculate the number of activated droplets from the simulated aerosol size distribution, composition, and meteorological conditions. Increasing N_d can impact the cloud droplet effective radius and therefore cloud albedo (ACI_α; Jones et al., 2001). Changes in N_d also modify the cloud lifetime and hydrological cycle (ACI_τ) through changes in the autoconversion of cloud liquid water to rain water, which is simulated in GA7 using the scheme of Khairoutdinov and Kogan (2000).

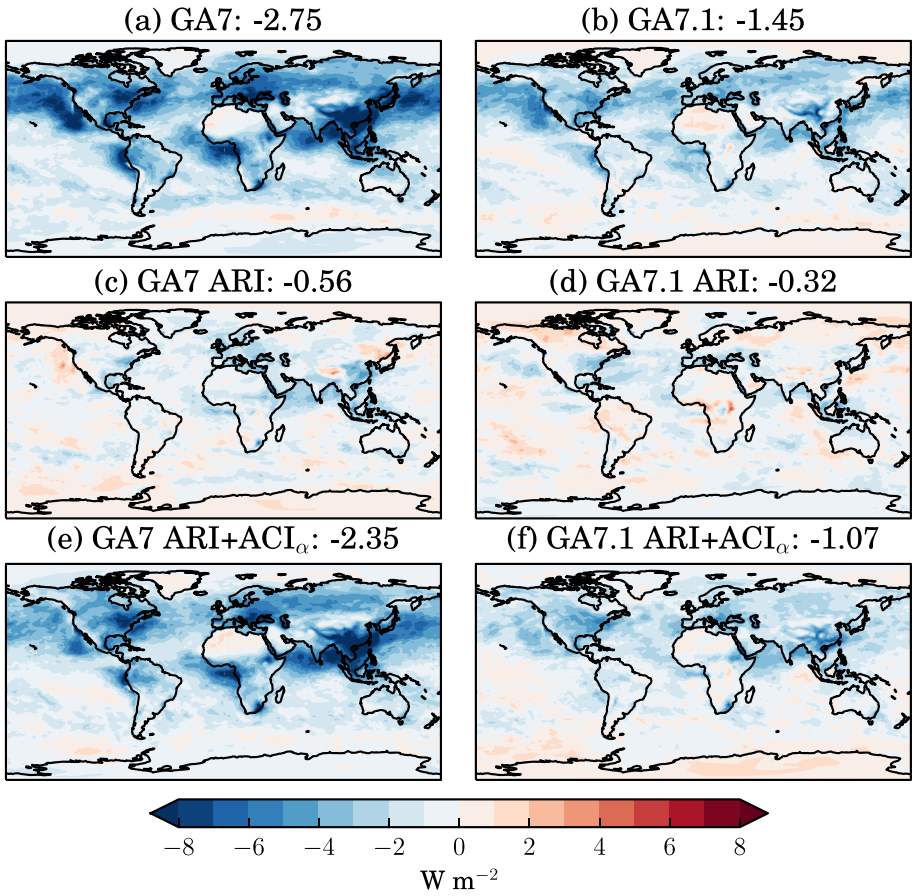

Figure 1. The aerosol effective radiative forcing due to (a, b) all aerosol-cloud-radiation interactions, (c, d) aerosol-radiation interactions only, and (e, f) aerosol-radiation plus aerosol-cloud albedo interactions only in (a, c, and e) GA7 and (b, d, and f) GA7.1 model configurations. The global mean aerosol effective radiative forcing values are shown in the title of each subpanel. ACI = aerosol-cloud interaction; ARI = aerosol-radiation interaction.

The aerosol ERF is defined here as the change in net top-of-atmosphere (TOA) radiation flux in a PI climate due to the perturbation of anthropogenic aerosol emissions only to PD values and follows the *fixed sea surface temperature* methodology outlined in Forster et al. (2016) and Pincus et al. (2016). Two 20 year climate model simulations are performed. Both set the forcing for sea-ice, sea surface temperatures, vegetation, greenhouse gases, and ozone to the year 1850. In the first simulation all aerosol emissions are set to the year 1850 (PI experiment) while in the second the anthropogenic aerosol emissions of sulphur dioxide (SO_2), black carbon (BC) and organic carbon (OC) are changed to the year 2000 (PD experiment). Emissions of aerosols and their precursors are taken from the CMIP5 database (Lamarque et al., 2010) and background volcanic SO_2 emissions prescribed from Andres and Kasgnoc (1998). The choice of running the simulations for 20 years as opposed to 30 years recommended in Forster et al. (2016) is based on the computational cost of running a large number of ERF simulation pairs (outlined in Table 1). We believe that the aerosol ERF estimates are robust as the standard error (reflecting the variability in the net radiation TOA flux) is relatively small (less than 0.06 W/m^2) in all cases.

Figure 1a shows the all-sky aerosol ERF in GA7. The global mean aerosol ERF is −2.75 W/m^2 (see also Table 1). This strong forcing is driven primarily by the large negative forcing across the Northern Hemisphere (NH) where anthropogenic aerosol emissions dominate. Aerosol source regions of China, eastern Europe, and northeastern United States show large regional forcings of up to −9 W/m^2, and this forcing appears to persist downwind of these sources across the North Pacific and Atlantic Oceans. Regions dominated by stratocumulus cloud off the western coasts of central Africa, South America, and California also show a strong negative forcing indicating a possible strong ACI. Also of interest is the apparent widespread negative forcing over much of the Southern Hemisphere (SH) oceans, a region that would largely be considered as pristine (Hamilton et al., 2014).

Table 1
Summary of Model Simulations Performed and the Corresponding Global Mean Aerosol and Total Anthropogenic Effective Radiative Forcing in 2000 Relative to 1850

Experiment	Description	ERF_{Aer} (W/m^2)	SE	ERF_{Anthro} (W/m^2)	PI NET_{TOA} (W/m^2)
GA7	GA7	−2.75	0.056	−0.60	0.86
GA7_ARI	GA7: ARI only	−0.56	0.043	—	−5.40
GA7_ARI_ACI_α	GA7: ARI + ACI_α only	−2.35	0.047	—	−0.72
GA7_dis	GA7 + revised cloud droplet spectral dispersion	−2.11	0.031	—	0.70
GA7_abs	GA7 + aerosol absorption updates	−2.45	0.043	—	1.32
GA7_act	GA7 + aerosol activation improvements	−2.56	0.048	—	1.88
GA7_dms	GA7 + DMSx1.7	−2.36	0.055	—	−0.37
GA7_comb	GA7 + GA7_dis + GA7_abs + GA7_act + GA7_dms	−1.37	0.053	—	0.59
GA7.1	GA7_comb + cloud tunings	−1.45	0.043	+0.75	−0.24

Note. Also included are the standard error, SE, of the aerosol ERF and the global mean PI net TOA radiative flux. ERF = effective radiative forcing; PI = preindustrial; ACI = aerosol-cloud interaction; ARI = aerosol-radiation interaction; TOA = top-of-atmosphere.

Parallel pairs of simulations enabling the ARI only (GA7_ARI) and the aerosol-radiation plus aerosol-cloud albedo interactions (GA7_ARI_ACI_α) only are also performed. In the GA7_ARI experiment the ERF due to ACIs is not included, such that prescribed N_d concentrations are held constant in both PI and PD simulations. In the GA7_ARI_ACI_α experiment the ERF due to the aerosol lifetime effect is suppressed by keeping N_d constant in the autoconversion process but allowing the cloud effective radius and cloud albedo respond to the changing aerosol concentrations. These experiments enable the separation of the different components of the total aerosol ERF. The aerosol ERF from the different model experiments is tabulated in Table 1. The global mean aerosol ERF due to ARI only is −0.56 W/m^2 (Figure 1c). This value is stronger than multimodel mean estimates reported to be in the range of −0.22 to −0.32 W/m^2 but is within the reported multimodel spread (Myhre, Samset, et al., 2013; Schulz et al., 2006). The global mean aerosol ERF due to ARI + ACI_α is −2.35 W/m^2 (Figure 1e). This large forcing indicates that the aerosol-cloud lifetime effect contribution to the total aerosol ERF is relatively small (15%) and highlights the large role of the cloud albedo response.

The net total aerosol ERF is well outside the 5–95% range of −1.9 to −0.1 W/m^2 reported by IPCC AR5 (Myhre, Shindell, et al., 2013). As a result of this large and negative forcing, the total anthropogenic ERF is computed to be −0.6 W/m^2. The GA7 model and by implication the HadGEM3-GC3 model are therefore not acceptable for inclusion in UKESM1. In the following section we explore uncertainties in a number of physical model processes and parameterizations, which are believed to have a significant impact on the aerosol ERF.

3. Model Developments

Given the realistic simulation of aerosols in the GA7 model (Walters et al., 2017) and the apparent large contribution of ACI_α to the total aerosol ERF (see section 2) our investigation focuses on missing or poorly represented processes that could lead to an excessively large negative aerosol ERF, in particular, parameterizations underpinning the aerosol-cloud-radiation interactions. Table 1 outlines all the model experiments carried out in this section. Below we detail and justify the model changes that were selected for inclusion in the final revised *branch* configuration of GA7, labeled GA7.1, and separately examine the impacts of each change on the total aerosol ERF. Our primary goal is to develop a model configuration that fulfills the positive total anthropogenic historical ERF criterion, while its PD climate should evaluate at least as well as GA7. The final GA7.1 configuration is evaluated in section 5.

3.1. Cloud Droplet Spectral Dispersion

The impact of aerosols on cloud albedo is a combination of (i) a cooling effect due to an increased number of smaller cloud droplets enhancing cloud reflectivity (Twomey, 1974) and (ii) a warming due to enhanced cloud droplet spectral dispersion (Liu & Daum, 2002; Lohmann & Feichter, 2005). A key parameter determining the cloud albedo response to aerosol perturbations is the cloud droplet effective radius, r_e, which, following Martin et al. (1994), can be written as follows:

$$r_e = \beta \sqrt[3]{\frac{3L}{4\pi\rho_w N_d}}, \tag{1}$$

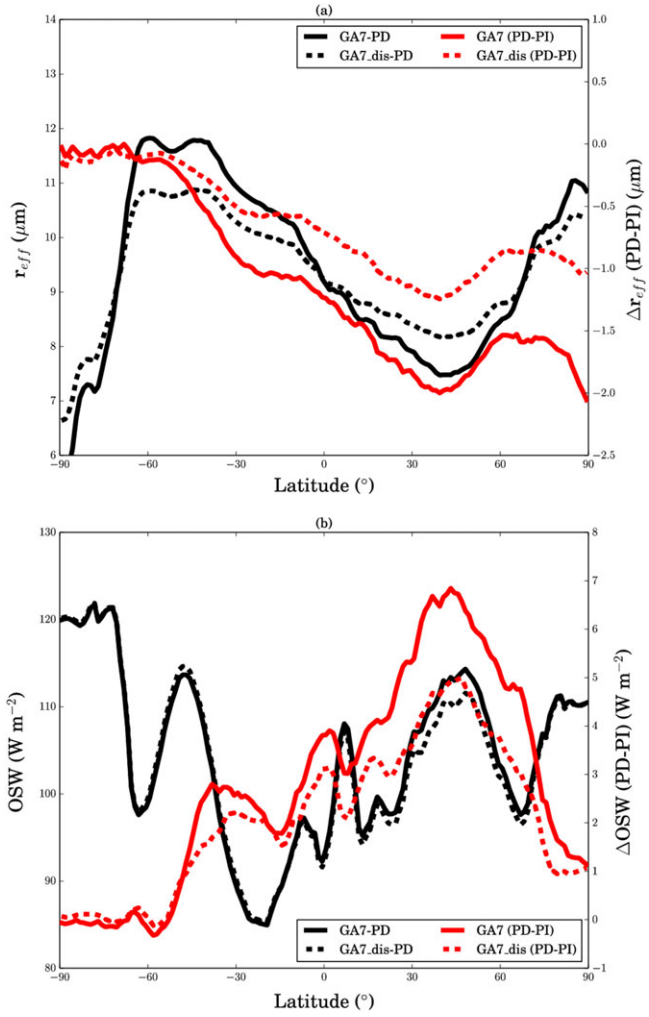

Figure 2. Impact of the updated cloud droplet spectral dispersion parameterization on zonal mean (a) cloud effective radius and (b) outgoing SW. Present-day values for GA7 (black solid lines) and GA7_dis (black dashed lines) simulations are shown along with the corresponding change from the preindustrial values (PD-PI, red solid and dashed lines). PD = present-day; PI = preindustrial; OSW = outgoing shortwave.

where L is the cloud liquid water content, ρ_w the liquid water density, N_d the cloud droplet number concentration, and β the spectral shape parameter. The β is an increasing function of the cloud droplet spectral dispersion, ϵ, defined as the ratio of the standard deviation to the mean radius of the cloud spectrum. Most GCMs do not accurately account for the dispersion effect and generally assume a constant value for β. Liu and Daum (2002) found ϵ (and therefore β) to be an increasing function of N_d, which offset the aerosol cooling effect by up to 80%. The degree of offset is dependent on the choice of parameterization of β (Liu et al., 2008; Peng & Lohmann, 2003; Rotstayn & Liu, 2003).

In GA7 the cloud droplet spectral dispersion is represented by two constants representing clean maritime ($\beta = 1.08$) and polluted continental ($\beta = 1.14$) air masses following Martin et al. (1994). A simple land-sea split is used to classify these regimes with clouds over land assumed to be continental and clouds over sea assumed to be maritime. Liu et al. (2008) examined the relationship of beta with both Nd and L. The resulting parameterization of β is as follows:

$$\beta = 0.07 \left(\frac{L}{N_d} \right)^{-0.14}. \quad (2)$$

Rotstayn and Liu (2009) found this representation of β weakened the first aerosol indirect effect by 42% in a GCM compared to a simulation using fixed β values in good agreement with the analytical estimates of Liu et al. (2008).

Figure 2a shows the zonal mean r_e from the standard GA7 PD simulations and equivalent simulations where β was parameterized following equation (2) (GA7_dis). In the PD simulation the revised β reduces the strong hemispheric asymmetry seen in r_e, increasing r_e in the anthropogenic aerosol dominated NH midlatitudes (large β) and reducing r_e in the more pristine maritime environments (small β) such as the SH (Figure 2a). This leads to a more reflective SH and less reflective NH, as shown in Figure 2b. Section 5 will highlight how this improves systematic model radiation biases.

It is clear from Figure 2a that the change in r_e due to the PD aerosol perturbation is much smaller in GA7_dis than in GA7 particularly in the NH. This leads to a concomitant smaller change in the outgoing shortwave (OSW) radiation (Figure 2b) due to a smaller cloud albedo response and a weaker aerosol forcing of 23% with a total aerosol ERF of −2.11 W/m^2. The change in aerosol ERF is less than the 42% reduction previously reported by Rotstayn and Liu (2009) and is likely model dependent, for example, individual models will have very different cloud climatologies.

3.2. Aerosol Absorption

In GA7 and earlier science configurations the refractive index of BC aerosol is based on World Climate Research Program (1986). Evaluation of GA7 against Aerosol Robotic Network (AERONET) ground-based measurements has shown an overall underestimation of the absorption aerosol optical depth (AAOD) and an overestimation of the single scattering albedo (SSA) in regions where aerosol absorption is dominated by anthropogenic emissions of BC (Mollard, 2017). To address this low bias, using recent evidence that reviews the optical properties for BC (Bond et al., 2013), the BC refractive index is updated to the middle estimate recommended by Bond and Bergstrom (2006). This increases the BC refractive index from 1.75−0.44i to 1.85−0.71i at 550 nm. A further technical change increases the spectral resolution of the look-up tables used in the calculation of the aerosol optical properties. This allows small values of the imaginary part of the refractive index to be resolved, further increasing the absorption in regions where the BC loading is relatively low. Together, these changes approximately double the absorption of solar radiation by BC. This is demonstrated in Figure 3, which shows the AAOD at 550 nm from two simulations which are identical apart from the change to BC optical properties.

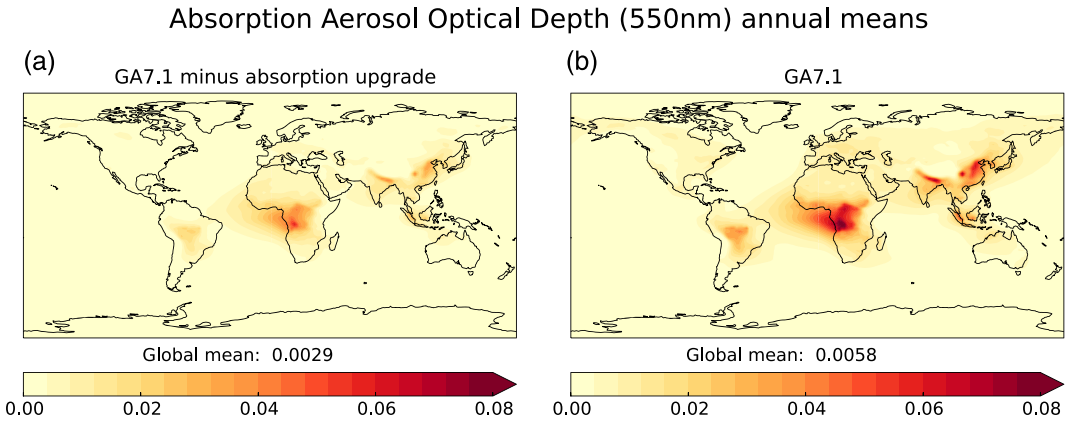

Figure 3. Absorption aerosol optical depth in (a) control simulation with old black carbon absorption properties and (b) simulation with new black carbon absorption updates included.

Modeled AAOD is enhanced everywhere, with the biggest increases in regions with heavy BC loadings such as South Asia, China, tropical Africa, and South America. The BC upgrades also mean that modest values of AAOD over Europe and North America are now resolved where they were previously (erroneously) virtually 0.

The increase in BC absorption leads to an increase in the net radiative flux at TOA in the PD by 0.54 W/m^2 and weakens the GA7 aerosol ERF by +0.30 W/m^2 leading to a revised global net aerosol ERF of −2.45 W/m^2.

3.3. Aerosol Activation

The activation of aerosol particles to cloud droplets is strongly related to the subgrid vertical velocity variance, σ_w, as well as the physical and chemical composition of the aerosols themselves. In GA7, σ_w is diagnosed in UKCA-Activate (West et al., 2014) as follows:

$$\sigma_w = \max\left(\sqrt{\frac{2}{3}\mathrm{TKE}_{\mathrm{BL}}}, \sigma_w^{\min}\right), \tag{3}$$

where the boundary layer turbulent kinetic energy ($\mathrm{TKE}_{\mathrm{BL}}$) is estimated from the model turbulent mixing scheme as follows:

$$\mathrm{TKE}_{\mathrm{BL}} = \frac{K_m}{\tau_{\mathrm{turb}}}, \tag{4}$$

where K_m is the eddy diffusivity for momentum and τ_{turb} a parameterized turbulent time scale (Walters et al., 2017). The $\sigma_w^{\min}$ is a prescribed minimum value, set to 0.1 m/s in GA7. This constant is used as both a numerical minimum and to represent TKE in regions where the turbulent mixing scheme is not the only source of subgrid TKE. The $\sigma_w^{\min}$ value was originally justified in GCMs with coarse vertical resolutions where cloud top turbulent forcing was not adequately resolved and there was no diagnosis of σ_w in convective updraughts. The vertical resolution has improved dramatically in the latest configurations of HadGEM3, which have 85 levels (50 of which are operated on by the turbulent mixing scheme) compared to the 38 levels used in the West et al. (2014) study. The enhanced vertical resolution negates the original requirement for such a high specified minimum value, the choice of which significantly impacts the number of activated particles and subsequent aerosol indirect forcing (Golaz et al., 2011). Indeed, West et al. (2014) note the high occurrence of $\sigma_w^{\min}$ in their simulations and highlighted the need for further evaluation.

First, a level indexing bug was found and corrected in the activation scheme, which in any grid cell was causing aerosol activation to be calculated using the value of TKE from the grid cell below. Because σ_w typically peaks in the midboundary layer, the effect of the bug was that TKE, and therefore aerosol activation, was underestimated below this level (near the surface) and overestimated above this level (in the free troposphere).

Second, as discussed in Boutle et al. (2018), the use of $\sigma_w^{\min} = 0.1$ m/s is particularly poor in stable boundary layers where turbulence is often very weak and following equation (3) leads to the application of a σ_w that is too high in these cases. Therefore, we follow the suggestions made in Boutle et al. (2018) and reduce $\sigma_w^{\min}$

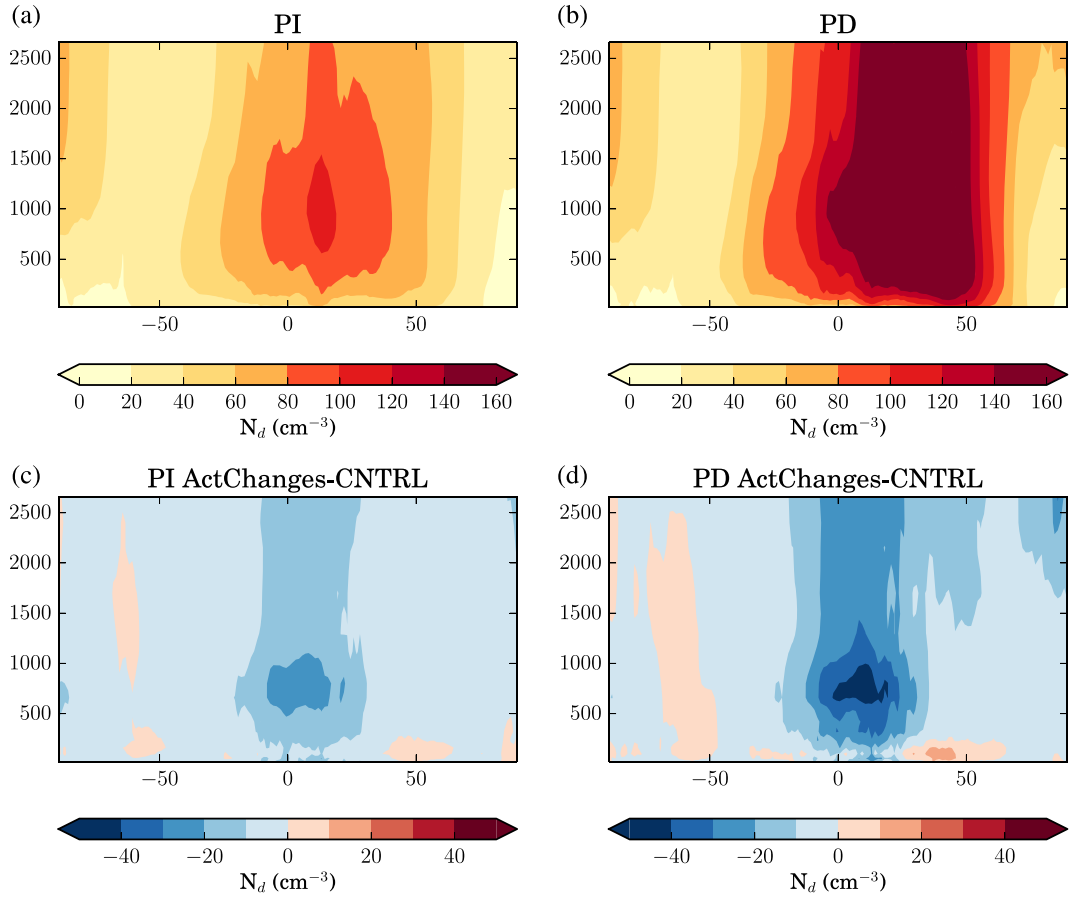

Figure 4. Zonal mean cloud droplet number concentrations (N_d) in the GA7 (a) preindustrial and (b) present-day simulation. The impact of aerosol activation improvements on zonal mean N_d distribution in the (c) PI, (d) PD periods. PD = present-day; PI = preindustrial.

to 0.01 m/s, which now represents a more genuine numerical minimum and is rarely triggered. As shown in Boutle et al. (2018), this gives a significant reduction in near-surface aerosol activation, primarily from low-level cloud in stable boundary layers, that is, fog. The reductions are also largest over polluted NH land masses.

Third, as noted previously and in West et al. (2014), the above change cannot be made without introducing an explicit estimate of TKE in convective cloud regimes where significant subgrid vertical velocity variance is present but is parameterized by the mass flux convection scheme and not by the turbulent mixing scheme and where therefore there is no diagnosis of TKE_{BL}. In these regimes, we assume that any vertical velocity leading to aerosol activation is due to the convective updraft, which by definition is given by

$$w_{\text{conv}} = \frac{M}{g\rho \text{CCA}}, \tag{5}$$

where M is the convective mass flux, CCA the convective cloud amount, g the acceleration due to gravity, and ρ the air density. Equation (3) above is then modified to

$$\sigma_w = \max\left(\sqrt{\frac{2}{3}\text{TKE}_{\text{BL}}}, w_{\text{conv}}, \sigma_w^{\min}\right). \tag{6}$$

and thus provides a direct link between the aerosol activation and the location and strength of convection.

Figure 4 shows the global zonal mean distribution of N_d from both the PI and PD simulations in GA7. The change in the distribution of N_d between the PI and PD periods is evident with a marked increase in N_d in the NH and a smaller relative increase in the SH tropics in the PD simulation. Notably, there is little change south of 50°S where anthropogenic influences are negligible (Hamilton et al., 2014). The impact of the revised diagnosis of σ_w (i.e., all three changes discussed above, GA7_act) for aerosol activation on the zonal vertical

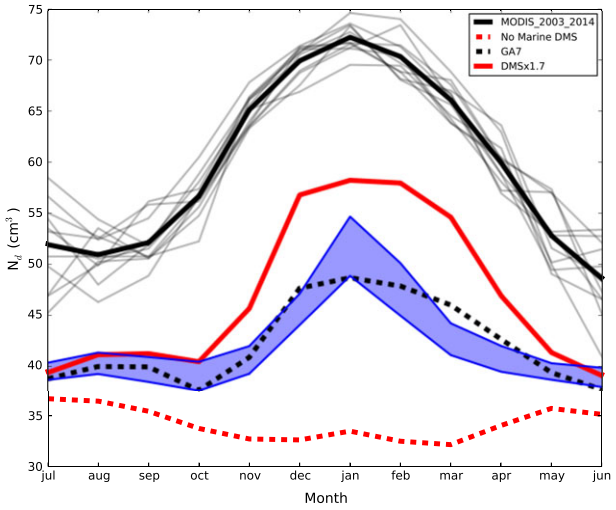

Figure 5. Seasonal cycle of N_d over the Southern Ocean (averaged between 35°S and 55°S) from GA7 (dashed black line) and GA7_dms (solid red line) simulations compared with satellite derived N_d from MODIS. The solid black line is the monthly mean MODIS N_d averaged from 2003 to 2014, while the light gray lines are the monthly data from each individual year. The blue shading represents uncertainty in N_d derived from uncertainty in the DMS seawater concentration as provided by Lana et al. (2011). *No Marine DMS* represents the contribution to N_d from non-DMS aerosol sources, primarily sea salt. DMS = dimethyl sulfide; MODIS = Moderate Resolution Imaging Spectroradiometer.

distribution of N_d for both simulations is also shown in Figure 4. The pattern of the changes is dominated by the level indexing bug fix and somewhat hides the effect of the two physical model improvements, which act to reduce N_d near the surface (as shown in Boutle et al., 2018) and increase N_d in the regions of strongest convective activity. Both periods show the same sign of difference although the differences are larger in the PD than in the PI period due to the higher N_d concentrations in the PD simulation. The combined changes weaken the aerosol ERF by +0.19 W/m^2, leading to an aerosol ERF of −2.56 W/m^2. Approximately half of this change is due to the bug fix and half due to the reduced $\sigma_w^{\min}$.

3.4. Natural Aerosol

Lack of knowledge of the PI aerosol base state is a key uncertainty in the aerosol ERF estimates. Carslaw et al. (2013) report that 45% of the variance in aerosol forcing is due to uncertainty in natural emissions of marine dimethyl sulfide (DMS), volcanic emissions of SO_2, biogenic volatile organic compounds, biomass burning, and sea spray. While sea salt and mineral dust aerosol are the largest contributors to the global aerosol load, the uncertainty in their global emissions spans orders of magnitude (Huneeus et al., 2011; Lewis & Schwartz, 2004). These emissions are highly model dependent, being sensitive to model resolution, wind speed, and land surface properties. Emission estimates of gaseous DMS from the ocean are derived from a limited set of ocean cruise measurements, which are then interpolated to make global emission data sets with large estimated uncertainty ranges of between 17.6 and 34.4 Tg[S] (Lana et al., 2011). Similarly models, such as Earth system models, which incorporate interactive DMS emissions, are weakly constrained due to sparsity in globally representative observations for validation (Halloran et al., 2010).

DMS-derived sulfate aerosol is known to be an important contributor to the global marine cloud condensation nuclei (CCN) distribution (Korhonen et al., 2008; Woodhouse et al., 2010). Recent studies also highlight the additional large contribution of biogenic aerosol from marine organic sources to the CCN population in pristine marine regions in both NH and SH (Meskhidze & Nenes, 2006; O'Dowd et al., 2004). McCoy et al. (2015) show that both DMS and marine organic sources are needed to explain discrepancies between observed and modeled N_d in the Southern Ocean and found that over 53% of the variance in N_d in this region was due to a combination of these two biogenic sources. Yet few GCMs incorporate any representation of marine organic sources.

Primary marine organic emissions show a high correlation with subsurface chlorophyll (Gantt et al., 2011; Rinaldi et al., 2013; Spracklen et al., 2008) in a similar manner to DMS (Anderson et al., 2000; Aranami & Tsunogai, 2004; Simò & Dachs, 2002). As a first step, we attempt to represent this missing aerosol source in the current model through enhancement of the parameterized ocean-atmosphere DMS flux and subsequent treatment of this increased aerosol in the GLOMAP-mode scheme. The marine DMS emissions are scaled by $DMS\times(1+0.7)$ where the additional 0.7 represents the missing organic source. Figure 5 evaluates the simulated PD seasonal cycle of N_d over the Southern Ocean (averaged between 35°S and 55°S) against Moderate Resolution Imaging Spectroradiometer (MODIS) satellite retrievals following McCoy et al. (2015), which was based on the N_d data set described in Grosvenor and Wood (2014). As McCoy et al. (2015) use only 1 year of MODIS observations we extend the evaluation to also include multiannual retrievals of MODIS N_d (Grosvenor et al., 2018) from 2003 to 2014. This better reflects the interannual variability in Southern Ocean N_d. For the analysis here the 2.1-μm effective radius values are used to compute N_d from MODIS. While acknowledging the large uncertainties in satellite retrievals of N_d (Grosvenor et al., 2018) and the sparsity of retrievals at high latitudes in winter months a distinct seasonal cycle in N_d over the Southern Ocean is observed. Peak concentrations occur in the austral summer months and coincide with peak marine biogenic emissions (McCoy et al., 2015). A parallel simulation that did not include marine DMS sources was conducted to isolate the non-DMS *background* contribution (primarily sea salt) to N_d in this region. While the background aerosol contribution

Table 2
Values of Tuned Parameters in GA7.1 and Original Values in GA7

Scheme	Variable	Description	GA7	GA7.1
Large-scale cloud	mp_dz_scal	scaling factor for the mixing length in mixed phased clouds	1.0	2.0
Convection	cca_sh_knob	fraction of diagnosed shallow convective cloud passed to the radiation scheme to represent the convective core	0.2	0.5

in GA7 is in good agreement with the 36 cm^{-3} reported by McCoy et al. (2015), the total N_d is largely underestimated. In particular, the peak N_d concentrations in austral summer are not captured demonstrating an underestimation of the biogenic contribution to the total N_d in the model. Scaling the DMS emissions clearly improves the agreement with MODIS, particularly in the summer period. Improvements in the PD evaluation of TOA outgoing SW radiation fluxes are also found (see section 5). The choice of scaling value is based on a balance of improving the seasonal cycle of N_d and the PD evaluation of TOA fluxes while also keeping the net TOA radiation balance within the required target range of 0 ± 0.5 W/m^2. Further increasing the scaling value would lead to a more negative net TOA radiation balance pushing it outside of this range in the final configuration (see section 4).

As part of the assessment of the natural aerosol emissions we also updated the prescribed DMS seawater concentrations from Kettle et al. (1999) to the more recent Lana et al. (2011) data set driving the marine DMS emissions. This relatively small update increases the DMS seawater concentration by 20% primarily in the tropics and was found to have only a very small impact on the aerosol ERF. Global uncertainty ranges supplied by Lana et al. (2011) are used to assess the resulting uncertainty in simulated N_d from the marine DMS source independently of any scaling (blue shading in Figure 5). From this it is evident that while the uncertainty in the DMS seawater concentrations can account for some of the underestimation of N_d, it does not account for all. Therefore, scaling the marine DMS emissions to account for missing organic sources is fully justified and leads to a significant improvement in the seasonal N_d cycles.

Through enhancement of the PI background CCN and subsequent N_d the DMS updates described above weaken the aerosol ERF by +0.39 W/m^2 leading to a global net aerosol ERF of −2.36 W/m^2. Recognizing the limitations of treating natural marine organic aerosols in this way ongoing developments include implementing an improved mechanistic treatment of the marine organic aerosol source function to replace the simple treatment here.

4. Defining the GA7.1 Configuration

The individual model developments described above are combined to define a branch of the GA7 configuration, termed GA7.1. As with the development of many GCMs, certain additional tunings are required to bring the net radiation at the TOA back into balance (Schmidt et al., 2017). Largely due to the redistribution of the N_d with the aerosol activation changes described in section 3.3 a retuning of two cloud parameters was required in GA7.1. These are the following:

1. the scaling factor for the mixing length in mixed phased clouds and
2. the fraction of diagnosed shallow convective cloud passed to the radiation scheme to represent the convective core.

Both of these parameters are described in Walters et al. (2017) and are tuned only within their estimated uncertainty. In both cases the parameters above are retuned back to the values recommended by the original literature describing the relevant model developments (Furtado et al., 2016; Grant & Lock, 2004) and brings the PI net TOA radiation balance to within the target range of 0 ± 0.5 W/m^2. The parameter values are summarized in Table 2.

The total aerosol ERF in the revised GA7.1 model configuration is −1.45 W/m^2 nearly 50% of its original value (see Table 1). The geographic distribution of the aerosol ERF is less negative across all regions of the globe compared with GA7 (Figure 1b). In particular, large changes are found in the stratocumulus cloud regions and anthropogenic source and outflow regions across the NH. The widespread negative ERF across the SH oceans

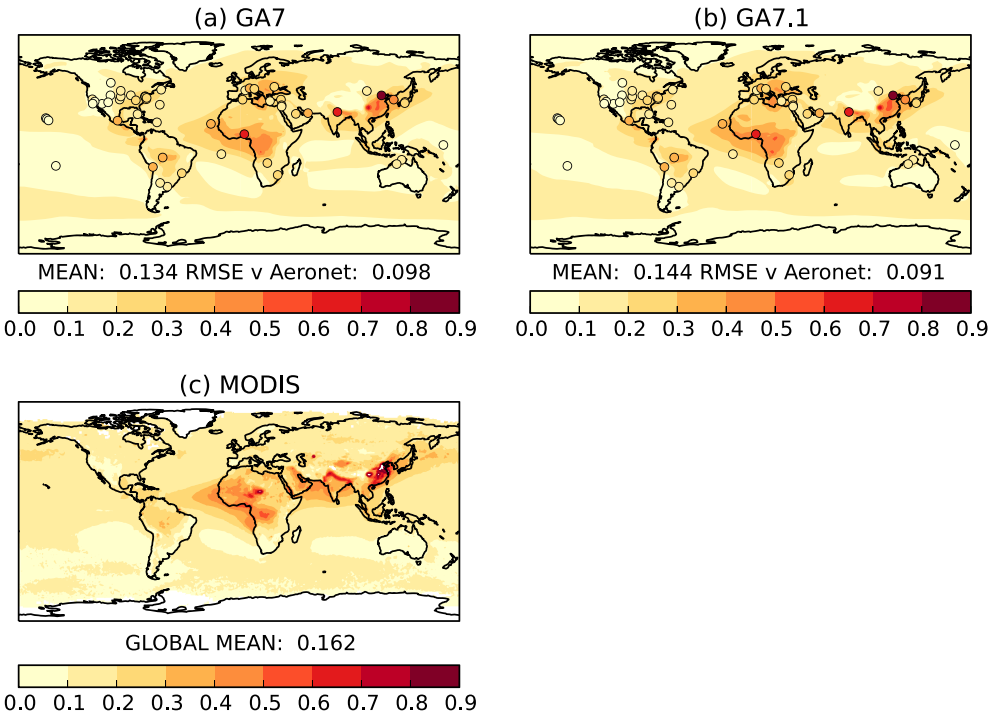

Figure 6. Annual mean aerosol optical depth at 550 nm from (a) GA7, (b) GA7.1 climate simulations, and (c) MODIS satellite observations. The MODIS satellite data are from collection 6 (Sayer et al., 2014) and represents an annual average from 2003 to 2012 inclusive. The circles in (a) and (b) show the annual mean AOD at various AERONET stations. MODIS = Moderate Resolution Imaging Spectroradiometer; RMSE = root-mean-square error; AERONET = Aerosol Robotic Network.

is also significantly weaker. The revised total aerosol ERF value falls within the IPCC AR5 estimated range for the total aerosol ERF (Myhre, Shindell, et al., 2013).

The GA7.1 global mean aerosol ERF due to ARI only and ARI + ACI_{α} is −0.32 and −1.07 W/m^2, respectively (Figures 1d and 1f). The aerosol ERF due to ARI is weaker than in GA7 and is in excellent agreement with the multimodel global mean estimate of aerosol ERF due to ARI of −0.27 W/m^2 (Myhre, Samset, et al., 2013). Aerosol-radiation feedbacks onto clouds result in the regions of positive forcing seen in Figure 1d.

This weaker aerosol ERF leads to a total anthropogenic ERF that is positive with a global mean value of +0.75 W/m^2 and thereby satisfies the requirement for acceptance for use in both UKESM and wider CMIP6 simulations with the HadGEM3-GC3.1 physical model. Below we evaluate the PD performance of the GA7.1 configuration relative to its parent GA7 reported by Walters et al. (2017).

5. Evaluation

A thorough evaluation of the GA7 science configuration is documented in Walters et al. (2017) and so we do not aim to repeat such an in-depth analysis here. Instead, we evaluate the impacts of the specific model developments outlined in section 3 in a 20-year free-running climate simulation driven by PD forcings and prescribed PD sea surface temperature and sea ice fields. Any notable changes relative to GA7 are compared against observations where possible. Overall, the impact of the changes implemented in GA7.1 is relatively small in a PD climate and where they do occur are found to be beneficial.

Figure 6 shows the global mean distribution of the aerosol optical depth (AOD) at 550 nm from GA7 and GA7.1 simulations. The global mean change in AOD from 0.13 to 0.14 is less than 10%. Increases in AOD are found primarily in the SH tropical oceans where the increase in DMS seawater concentration (and subsequent flux enhancement of DMS to the atmosphere) due to the Lana et al. (2011) climatology is largest. Enhanced marine DMS emissions due to the DMS scaling also lead to increases further south in the Southern Ocean. Qualitatively, both configurations agree equally well with satellite retrieved AOD from MODIS (Figure 6c) and the GA7.1 global mean of 0.14 is in better agreement with the MODIS global mean value of 0.16. Both model configurations overestimate AOD across eastern Europe and underestimate dust AOD over the Sahara and across the Arabian Sea. AOD over Southeast Asia, India, and China is also underrepresented in the models but

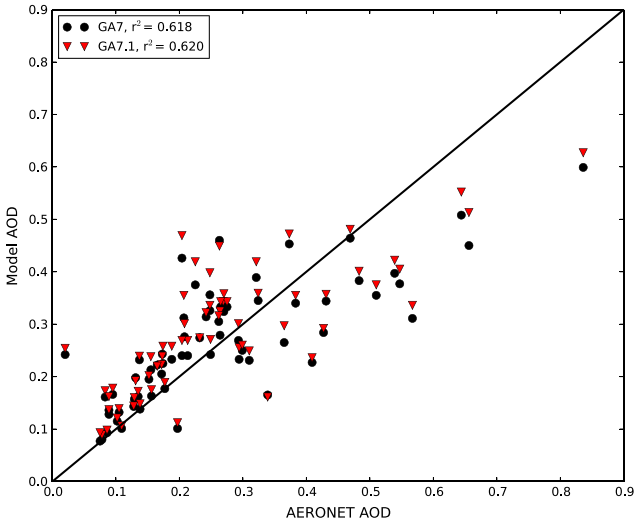

Figure 7. Scatterplot of annual mean AOD at 440 nm from GA7 and GA7.1 simulations against 67 global ground-based AERONET stations. AERONET = Aerosol Robotic Network; AOD = Aerosol optical depth.

increases in GA7.1 primarily through the updates to the BC absorption lead to small improvements in these regional biases. Remaining biases in these regions are believed to be due to uncertainties in the prescribed aerosol emissions and due to the use of emissions from the year 2000 in the model simulations, while the satellite observations are a multiyear mean from 2003 to 2012. An annual mean climatology of ground-based AOD measurements from the global AERONET (Holben et al., 2001) is overlaid on the global maps of simulated AOD in Figure 6 and is also more quantitatively compared in Figure 7. In general, the model captures well the regional variation in AOD although the higher AOD in GA7.1 slightly increases positive biases at a small number of sites (Figure 7). Nevertheless, the global root-mean-square error (RMSE) between the colocated model and AERONET AOD is reduced in GA7.1, while the correlation is improved.

The primary impact of the BC absorption is through the AAOD and the SSA. Figure 8 compares the monthly mean simulated AAOD with AAOD retrievals from AERONET (Dubovik & King, 2000; Dubovik et al., 2006). In Figure 8 the relative model bias is calculated as the mean of log(AAODmodel/AAODobs) to give equal weighting to biases at high and low AAOD values. The BC absorption upgrades in GA7.1 lead to marked improvements in this comparison with low biases in modeled AAOD greatly reduced and a narrowed distribution of modeled AAOD leading to far fewer severe underestimations. The increased absorption also leads to notable decreases in SSA generally improving agreement with AERONET SSA retrievals in most regions outside of regions strongly affected by biomass burning (not shown). A more detailed analysis is included in Mollard (2017).

Global distributions of N_d are shown in Figure 9. The global mean change in cloud top N_d is also within 10% with a decrease in global mean N_d from 114 to 106 cm^{-3}. However, the small global mean decrease in GA7.1 masks larger opposing hemispheric changes shown in Figure 9f. Reducing the value of σ_w^{min} in the aerosol activation scheme described in section 3.3 leads to widespread reduction in N_d across the NH and global land masses. While in the SH, higher emissions of marine DMS dominate the impacts found and N_d is generally increased over the ocean. In particular, the stratocumulus regions in the Southeast Pacific and Southeast Atlantic show increases of up to 30%. While there are uncertainties associated with global remotely sensed N_d distributions from satellites (Grosvenor et al., 2018), which limits their quantitative application to directly evaluate modeled N_d we can qualitatively assess the global distributions of N_d. Figure 9 compares the global annual mean N_d at cloud top from both GA7 and GA7.1 with N_d retrieved from MODIS using two different retrieval algorithms covering the years 2003–2015. Figure 9a shows the global MODIS N_d climatology described in Grosvenor and Wood (2014) and Grosvenor et al. (2018) and retrieves N_d over both land and

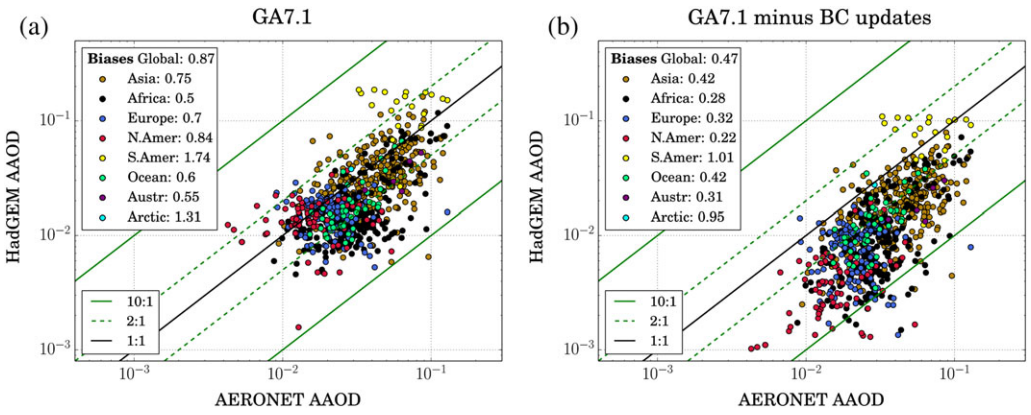

Figure 8. Impact of updated absorption properties on the validation of model AAOD against AERONET observations from 2006 to 2008 from 186 worldwide AERONET sites: (a) GA7.1 configuration and (b) GA7.1 with absorption updates removed. Data points are segregated into broad world regions. Relative biases are listed in the legend. AAOD = absorption aerosol optical depth; AERONET = Aerosol Robotic Network; BC = black carbon.

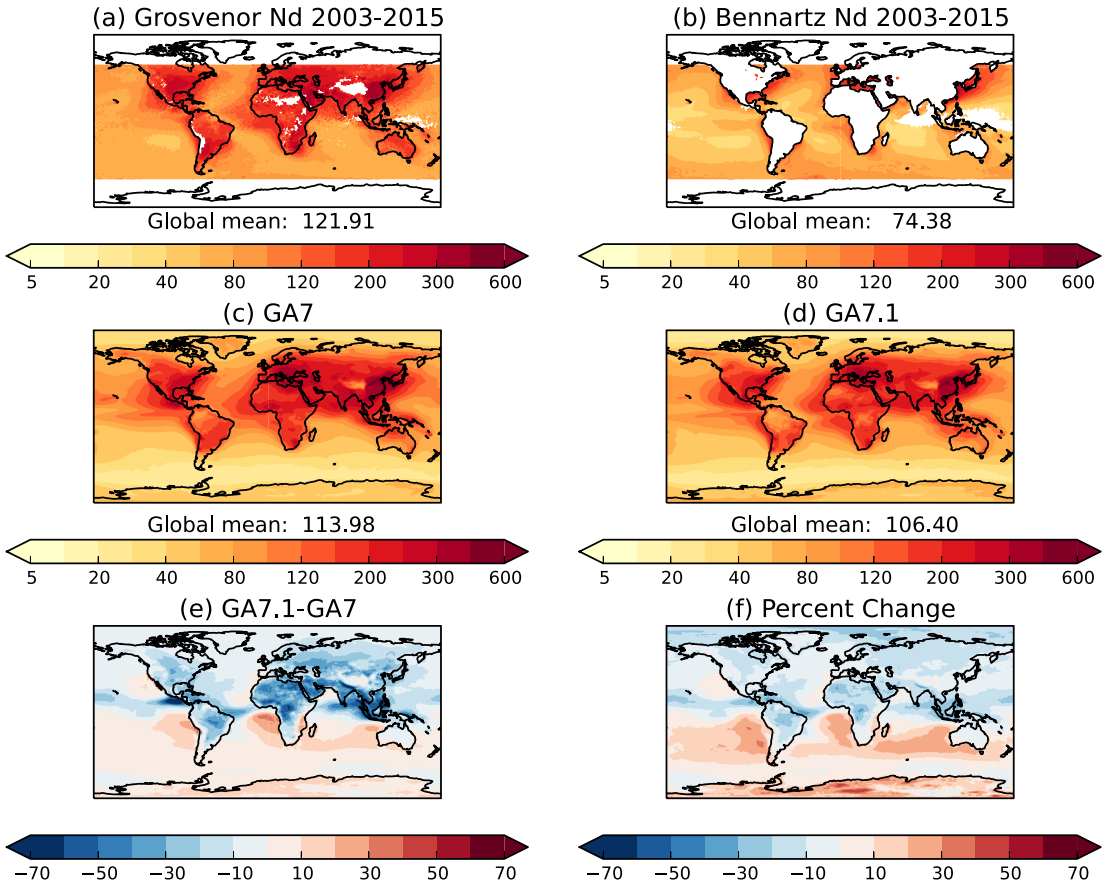

Figure 9. Observed and simulated annual mean N_d. MODIS retrieved N_d from years 2003–2015 using (a) Grosvenor et al. (2018) and (b) Bennartz and Rausch (2017) retrieval algorithms. Simulated cloud top N_d from (c) GA7, (d) GA7.1 simulations, (e) GA7.1-GA7 difference, and (f) GA7.1-GA7 percentage change. MODIS = Moderate Resolution Imaging Spectroradiometer.

ocean, while the Bennartz and Rausch (2017) N_d (Figure 9b) climatology retrieves information over ocean only. Retrieved data have been removed north of 60°N and south of 60°S where retrievals are most uncertain. The simulated N_d distributions from GA7 and GA7.1 are in very good agreement with Grosvenor et al. (2018) with highest N_d concentrations over land and downwind of key source regions. The stratocumulus cloud regions also appear well represented although N_d is lower in this region in Bennartz and Rausch (2017). Notwithstanding, the differences in the satellite data sets both have higher N_d across the Southern Ocean than in GA7, with this low bias being somewhat improved in GA7.1. Reductions in N_d over the NH oceans in GA7.1 are beneficial in reducing the positive bias seen in GA7.

The impact of the GA7.1 developments on the TOA outgoing SW (OSW) and LW (OLR) radiation fluxes are shown in Figure 10. The largest changes are seen in the OSW and are driven primarily by the changes in N_d highlighted above and subsequent feedback onto cloud properties. Figure 10c shows the GA7 bias in OSW when compared with CERES-EBAF (Clouds and the Earth's Radiant Energy System-Energy Balance and Filled dataset, Loeb et al., 2009). The model systematically overestimates the OSW in the NH and underestimates the OSW in the SH particularly in the stratocumulus regions of the Southeast Pacific and South Atlantic as well as in the Southern Ocean. Such large biases in the Southern Ocean lead to significant warm sea surface temperature biases in this region when coupled to an ocean model (Bodas-Salcedo et al., 2012; Hyder et al., 2018). In GA7.1, in the NH, the combination of lower N_d and enhanced cloud droplet spectral dispersion increases the cloud r_{eff} reducing the cloud albedo. The resulting reduction in OSW at TOA leads to improved agreement with CERES-EBAF (Figure 10e). In the SH the lower cloud droplet spectral dispersion and subsequent reduction in r_{eff} are further amplified by the increase in N_d in response to the increased DMS emissions. A modest increase (less than 15%) in the cloud liquid water path over the Southern Ocean is found due to both the DMS changes and mixed phase cloud tuning. The overall result is an increase in OSW of up to 10 W/m^2 over

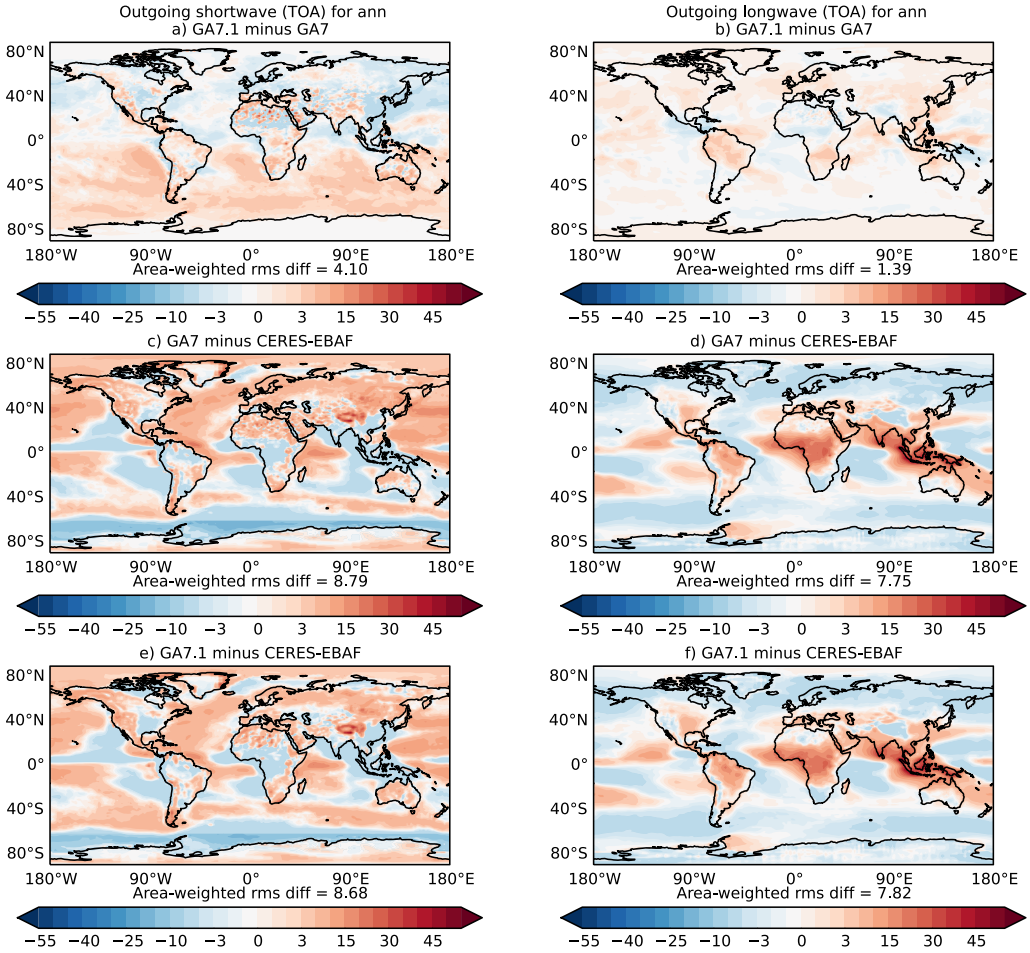

Figure 10. Assessment of annual mean outgoing (a, c, and e) shortwave and (b, d, and f) outgoing longwave radiation fluxes at top-of-atmosphere (TOA) (a, b) GA7.1-GA7 difference, (c, d) GA7 bias versus CERES-EBAF (Loeb et al., 2009), and (e, f) GA7.1 bias versus CERES-EBAF. CERES-EBAF = Clouds and the Earth's Radiant Energy System-Energy Balance and Filled dataset.

most of the Southern Ocean with even larger increases of up to 15 W/m^2 found in the stratocumulus cloud region in the Southeast Pacific. The opposing hemispheric changes in OSW lead to a much reduced asymmetry in the hemispheric OSW, with the NH-SH OSW difference reduced from 4.69 W/m^2 in GA7 to 1.50 W/m^2 in GA7.1. This increased hemispheric symmetry is closer to the latest observed values (Voigt et al., 2013). The NH-SH OSW gradient is increasingly seen as an important and fundamental part of the fully coupled climate system (Haywood et al., 2016; Stephens et al., 2016). Changes in OLR are overall much smaller than changes in OSW (Figure 10b). There is a general trend of higher OLR over most regions. In the NH these increases tend to improve negative biases in this regions, while increases in tropical land regions lead to small degradations in existing positive biases.

Figure 11 is analogous to Figure 12 in Walters et al. (2017) and summarizes the performance of GA7.1 compared to GA7 for a range of tropospheric fields, including pressure at mean sea level, temperature, precipitation, and wind fields. The performance metrics (representing the ratio of the RMSE of GA7.1 relative to GA7 for each variable) and observations used are described in Walters et al. (2017) and reflect the large-scale model response to the combination of model changes in GA7.1. Overall, nearly all metrics of global temperature, pressure at mean sea level, humidity, zonal wind, and precipitation fields show reductions in their RMSEs (indicated by green circles) with some small degradations found in tropical precipitation and horizontal wind performance (indicated by red circles), but these degradations are found to be small compared to internal climate variability.

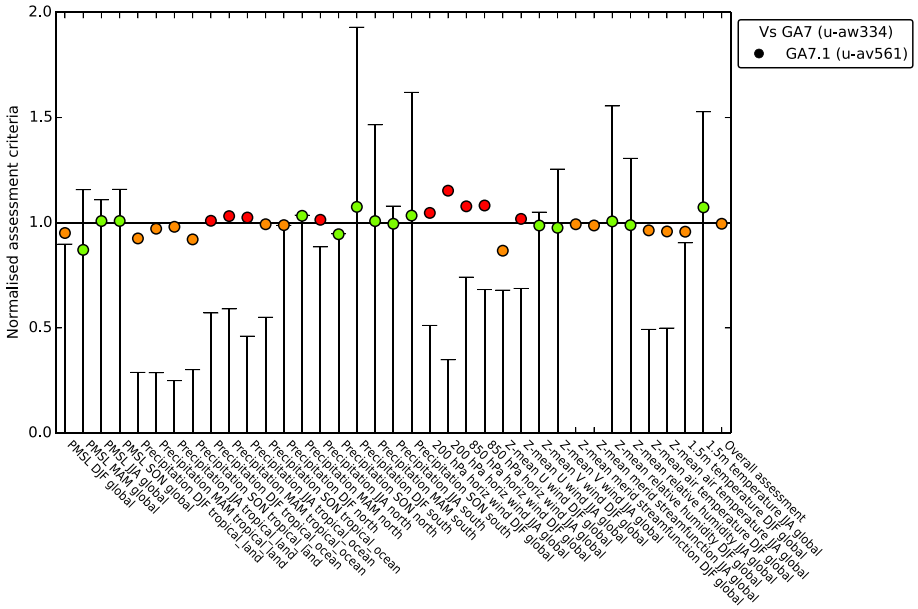

Figure 11. Normalized assessment criteria (ratio of RMSEs) for a number of global and regional atmospheric fields in GA7.1 compared to GA7. Details of the different observational data sets used for the calculation of the RMSE are given in Walters et al. (2017). Green circles denote fields with an improved RMSE within observational uncertainty (given by the whisker bars); orange and red circles denote improved and degraded RMSE, respectively, but where the RMSE lies outside of observational uncertainty. RMSE = root-mean-square error; DJF = December–February; MAM = March–May; JJA = June–August; SON = September–November. ; PMSL = pressure at mean sea level.

Overall, the evaluation of the GA7.1 configuration shows that the change in PD performance relative to GA7 is generally small across most standard tropospheric climate metrics. In areas of key change, such as the representation of the aerosol properties themselves and subsequent feedbacks onto clouds and radiation, GA7.1 generally validates better than GA7; PMSL = pressure at mean sea level.

6. Discussion

A strong, negative aerosol ERF was found in the latest Global Atmosphere configuration of the HadGEM3 climate model, GA7. While aerosols are known to offset a portion of the warming due to greenhouse gases, a total aerosol ERF of −2.75 W/m^2 implies a negative total anthropogenic ERF and therefore very likely a global climate cooling over the twentieth century in contradiction of observed temperature records. To minimize this risk, we require the aerosol ERF to be such that the total anthropogenic ERF is greater than 0 W/m^2. The occurrence of a negative anthropogenic ERF in GA7 triggered the work described in this paper. In this work we explore the sensitivity of the aerosol ERF to known shortcomings in the aerosol processes and the representation of aerosol-cloud-radiation interactions in the GA7 model. Guided by observational constraints of PD model performance, we develop an updated model, GA7.1, that included a number of either new or updated processes. GA7.1 has an aerosol ERF that is weaker by nearly 50% of the original GA7 value.

The largest single model change impacting the aerosol ERF is the inclusion of an improved cloud droplet spectral dispersion parameterization, a process largely ignored in most GCMs. The change reduces the aerosol-cloud albedo forcing and weakens the net aerosol ERF by +0.64 W/m^2. There is an increasing body of literature (Liu & Daum, 2002; Liu et al., 2008; Lohmann & Feichter, 2005; Peng & Lohmann, 2003; Rotstayn & Liu, 2003; Xie & Liu, 2013) highlighting the potentially important role of this process in ACIs and its ability to explain the lack of significant hemispheric differences in cloud brightness (Liu et al., 2008; Schwartz, 1998). Indeed, here we find significant improvement in the asymmetric hemispheric biases in GA7 when this process is included.

The second largest impact on the aerosol ERF is the inclusion of a simple representation of a primary marine organic aerosol source through the scaling of the marine DMS emission source. We recognize there are limitations with this method. For instance, the additional DMS emission is subsequently treated within the aerosol sulfur cycle and is oxidized to form sulfate aerosol as opposed to being treated as OC. This treatment is a

first step toward implementing a more physically based treatment of primary marine organic aerosol and its subsequent treatment in the final UKESM1 model. In the interim, for the physical model, we argue that this first step in accounting for this missing source is essential for improved N_d and OSW distributions. This is evidenced through improvements in the seasonal cycle of N_d in the pristine environment of the Southern Ocean and significant reductions in OSW biases.

Due to the strong control of natural emission on the PI baseline climate, we also examine the role of natural aerosol and associated uncertainty in emissions more generally. Emissions of both DMS and sea salt (not shown) have a large impact on PD TOA radiation fluxes and the aerosol ERF. For instance, additional tests with the GA7 model reveal the choice of air-sea DMS flux parameterization leads to variations in the aerosol ERF of up to 20% while independently scaling the total marine DMS emission by up to a factor of 2 changes the aerosol ERF by up to 40% (not shown). Wilcox et al. (2015) found the aerosol ERF sensitivity to variations in the PI sulfate load was much larger than to changes in sulfate load over the historical period in the CMIP5 models. This highlights the potentially larger role of natural marine sources over anthropogenic emissions in modulating global climate forcing and highlights the urgent requirement for improved observational and process-level understanding on the magnitude of these sources.

Changes to the aerosol activation and BC absorption properties, while smaller in terms of their relative impact on the aerosol ERF, are clear improvements to the way these processes are represented in the model. While more advanced interactive aerosol activation parameterizations, like that of Abdul-Razzak and Ghan (2000), have significantly improved our ability to simulate global distributions of PD N_d (West et al., 2014), the response of N_d (and hence aerosol ERF) to aerosol changes over the historical period is sensitive to the choice of parameterization of N_d (Rothenberg et al., 2017; Storelvmo et al., 2009). In UKCA-Activate, West et al. (2014) found the choice of treatment of the updraft velocity variance, σ_w, led to a spread of up to 0.4 W/m^2 in the aerosol ERF. Regayre et al. (2018) also find σ_w is an important source of the aerosol-cloud ERF uncertainty when they perturb a wide range of atmospheric and aerosol parameters in an earlier configuration of HadGEM3. Rather than prescribing fixed values of σ_w, which would not be globally representative, this work implements physically based improvements to the current σ_w treatment in UKCA-Activate and improves the robustness of the code. These improve our ability to simulate PD N_d climatology and lead to improved confidence in the historical change in N_d.

Fundamentally, even though the aerosol ERF of the GA7 and GA7.1 model configurations differs by 1.30 W/m^2, the simulated PD climate is remarkably similar and evaluates equally well across a wide range of standard performance metrics. This problem is not unique to the HadGEM3 model; for example, Golaz et al. (2013) document a similar issue in the Geophysical Fluid Dynamics Laboratory climate model. By tuning a number of cloud parameters, including the autoconversion threshold, cloud erosion time scales and σ_w^{min}, within plausible ranges Golaz et al. (2013) demonstrate a wide range in aerosol-cloud forcing but equally plausible PD climates. Interestingly, the choice of parameters that most accurately reproduced the observed twentieth century warming performs worst when compared against satellite observations of warm rain processes (Suzuki et al., 2017). This highlights a discrepancy between *top-down* and *bottom-up* approaches to model evaluation, the existence of model compensating errors and calls for further improved process-based assessment of climate models. This presents a key challenge for the climate model community as we enter into CMIP6. The ability of a GCM to simulate the observed change in historical global mean surface temperature is seen as a critical measure of a models ability to predict future climate change. This inevitably leads to the sometimes undesirable but often pragmatic approach of climate model tuning with many GCMs directly tuning the aerosol indirect effects (Hourdin et al., 2017; Schmidt et al., 2017). Given the large uncertainties in the aerosol-cloud forcing reported here and elsewhere, this practice is not surprising. Increasingly complex GCMs are developed using primarily PD observations, but the observations themselves provide little constraint on the aerosol ERF. Smarter exploitation of observations, through, for example, use of emergent constraints, is required. Recent novel techniques using PD aerosol-cloud relationships to inform changes since the PI period offer promise (Gryspeerdt et al., 2016, 2017; Malavelle et al., 2017). Furthering our understanding of natural aerosol processes that underpin the PI climate is also key to increasing our confidence in the GCMs ability to simulate historical and future climate change (Carslaw et al., 2017).

Table A1
Summary of UM Versions and Simulation Identifiers of All Simulations Used in This Study

Experiment	UM version	PI	PD	AMIP
GA7	UM10.6	u-aj944	u-aj996	u-aw334
GA7_ARI	UM10.6	u-au336	u-au337	
GA7_ARI_ACI$_\alpha$	UM10.6	u-au338	u-au339	
GA7_dis	UM10.6	u-ak001	u-ak002	
GA7_abs	UM10.6	u-ak004	u-ak005	
GA7_act	UM10.6	u-ak006	u-ak007	
GA7_dms	UM10.6	u-ak009	u-ak010	
GA7_comb	UM10.6	u-ak017	u-ak018	
GA7.1	UM10.6	u-ak019	u-ak020	u-av561

Note. PD = present-day; PI = preindustrial; AMIP = Atmospheric Model Intercomparison Project.

7. Conclusions

The HadGEM3-GA7 climate model was originally developed as the core physical atmosphere of the UKESM1. While this model evaluates well against PD observations, our analysis reveals an unrealistic large, negative aerosol ERF of −2.75 W/m^2. Such a large aerosol forcing would result in a significant global cooling in a coupled historical simulation, which is not supported by observations or models and the model was therefore deemed unacceptable for use in UKESM1.

Here we present an in-depth investigation into the uncertainties in the underpinning aerosol and physical model processes that lead to this overly strong aerosol forcing. We implement of a number of scientific model improvements in a new model configuration labeled GA7.1. The aerosol ERF in GA7.1 is −1.45 W/m^2 nearly 50% weaker than in GA7. The model developments are the following:

1. Implementation of an improved treatment of cloud droplet spectral dispersion used in the calculation of cloud effective radius;
2. Implementation of improvements to the aerosol activation scheme, UKCA-Activate, including an improved diagnosis of subgrid updraft velocity variance that enables the use of a reduced, more realistic numerical lower limit;
3. An update to the absorption optical properties for BC and increasing the spectral resolution of the look-up tables used in the calculation of the ARIs;
4. Implementation of a simple scaling of marine DMS emissions to account for missing primary marine organic aerosol source; and
5. An update to the DMS seawater concentration to the more up-to-date Lana et al. (2011) data set.

The PD climate of the new GA7.1 model evaluates equally well, if not better, than its GA7 parent. In particular, systematic biases in radiation fluxes are significantly improved. The more realistic aerosol ERF in GA7.1 leads to a net positive total anthropogenic ERF and is therefore acceptable for use in UKESM1. GA7.1 and its global coupled counterpart HadGEM3-GC3.1 form the physical model basis of UKESM1 and will be used extensively in CMIP6.

Acknowledgments
This work was primarily supported by the Met Office Hadley Centre Climate Programme funded by BEIS and Defra. C. J. and S. T. R. were jointly funded by the National Environmental Research Council (NERC) national capability grant for the UK Earth System Modelling project, grant NE/N017951/1 and the EU Horizon 2020 Research Programme CRESCENDO project, grant agreement 641816. The simulation data used in this study are archived at the Met Office and are available for research purposes through the JASMIN platform (www.jasmin.ac.uk) maintained by the Centre for Environmental Data Analysis (CEDA); for details please contact UM_collaboration@metoffice.gov.uk referencing this paper. Information on the exact model versions and simulation identifiers are provided in Table A1.

Appendix A: Data Availability

All simulation data used in this study are archived at the Met Office and are available for research purposes through the JASMIN platform (www.jasmin.ac.uk). For details please contact UM_collaboration@metoffice.gov.uk referencing this paper. Table A1 lists the model simulation identifiers for all model experiments presented in this study.

References

Abdul-Razzak, H., & Ghan, S. J. (2000). A parameterization of aerosol activation: 2. Multiple aerosol types. *Journal of Geophysical Research*, *105*, 6837–6844. https://doi.org/10.1029/1999JD901161

Anderson, T. R., Spall, S. A., Yool, A., Cipollini, P., Challenor, P. G., & Fasham, M. J. R. (2000). Global fields of sea surface dimethylsulfide predicted from chlorophyll, nutrients and light. *Journal of Marine Systems*, *30*, 1–20.

Andres, R. J., & Kasgnoc, A. D. (1998). A time-averaged inventory of subaerial volcanic sulfur emissions. *Journal of Geophysical Research*, *103*, 25,251–25,261. https://doi.org/10.1029/98JD02091

Andrews, T. (2014). Using an AGCM to diagnose historical effective radiative forcing and mechanisms of recent decadal climate change. *Journal of Climate*, *27*(3), 1193–1209. https://doi.org/10.1175/JCLI-D-13-00336.1

Andrews, T., Betts, R. A., Booth, B. B. B., Jones, C. D., & Jones, G. S. (2017). Effective radiative forcing from historical land use change. *Climate Dynamics*, *48*(11), 3489–3505. https://doi.org/10.1007/s00382-016-3280-7

Aranami, K., & Tsunogai, S. (2004). Seasonal and regional comparison of oceanic and atmospheric dimethylsulfide in the northern North Pacific: Dilution effects on its concentration during winter. *Journal of Geophysical Research*, *109*, D12303. https://doi.org/10.1029/2003JD004288

Bellouin, N., Mann, G. W., Woodhouse, M. T., Johnson, C., Carslaw, K. S., & Dalvi, M. (2013). Impact of the modal aerosol scheme GLOMAP-mode on aerosol forcing in the Hadley centre global environmental model. *Atmospheric Chemistry and Physics*, *13*(6), 3027–3044. https://doi.org/10.5194/acp-13-3027-2013

Bennartz, R., & Rausch, J. (2017). Global and regional esitmates of warm cloud droplet number concentration based on 13 years of AQUA-MODIS observations. *Atmospheric Chemistry and Physics*, *17*, 9815–9836. https://doi.org/10.5194/acp-17-9815-2017

Bodas-Salcedo, A., Williams, K. D., Field, P. R., & Lock, A. P. (2012). The surface downwelling solar radiation surplus over the Southern Ocean in the Met Office model: The role of midlatitude cyclone clouds. *Journal of Climate*, *25*(21), 7467–7486. https://doi.org/10.1175/JCLI-D-11-00702.1

Bond, T. C., & Bergstrom, R. W. (2006). Light absorption by carbonaceous particles: An investigative review. *Aerosol Science and Technology*, *40*, 27–67. https://doi.org/10.1080/02786820500421521

Bond, T. C., Doherty, S. J., Fahey, D. W., Forster, P. M., Berntsen, T., DeAngelo, B. J., et al. (2013). Bounding the role of black carbon in the climate system: A scientific assessment. *Journal of Geophysical Research: Atmospheres*, *118*, 5380–5552. https://doi.org/10.1002/jgrd.50171

Boucher, O., Randall, D., Artaxo, P., Bretherton, C., Feingold, G., Forster, P., et al. (2013). Clouds and aerosols. In O. Boucher, et al. (Eds.), *Climate Change 2013—The Physical Science Basis* (pp. 571–658). Cambridge, UK: Cambridge University Press.

Boutle, I., Price, J., Kudzotsa, I., Kokkola, H., & Romakkaniemi, S. (2018). Aerosol-fog interaction and the transition to well-mixed radiation fog. *Atmospheric Chemistry and Physics*, *18*, 7827–7840.

Carslaw, K. S., Boucher, O., Spracklen, D. V., Mann, G. W., Rae, J. G. L., Woodward, S., & Kulma la, M. (2010). A review of natural aerosol interactions and feedbacks within the Earth system. *Atmospheric Chemistry and Physics*, *10*(4), 1701–1737. https://doi.org/10.5194/acp-10-1701-2010

Carslaw, K. S., Gordon, H., Hamilton, D. S., Johnson, J. S., Regayre, L. A., Yoshioka, M., & Pringle, K. J. (2017). Aerosols in the pre-industrial atmosphere. *Current Climate Change Reports*, *3*(1), 1–15. https://doi.org/10.1007/s40641-017-0061-2

Carslaw, K. S., Lee, L. A., Reddington, C. L., Pringle, K. J., Rap, A., Forster, P. M., et al. (2013). Large contribution of natural aerosols to uncertainty in indirect forcing. *Nature*, *503*, 67. https://doi.org/10.1038/nature12674

Dubovik, O., & King, M. D. (2000). A flexible inversion algorithm for retrieval of aerosol optical properties from sun and sky radiance measurements. *Journal of Geophysical Research*, *105*, 20,673–20,696.

Dubovik, O., Sinyuk, A., Lapyonok, T., Holben, B. N., Mishchenko, M., Yang, P., et al. (2006). Application of spheroid models to account for aerosol particle nonsphericity in remote sensing of desert dust. *Journal of Geophysical Research*, *111*, D11208. https://doi.org/10.1029/2005JD006619

Eyring, V., Bony, S., Meehl, G. A., Senior, C. A., Stevens, B., Stouffer, R. J., & Taylor, K. E. (2016). Overview of the Coupled model Intercomparison Project Phase 6 (CMIP6) experimental design and organization. *Geoscientific Model Development*, *9*(5), 1937–1958. https://doi.org/10.5194/gmd-9-1937-2016

Forster, P. M., Richardson, T., Maycock, A. C., Smith, C. J., Samset, B. H., Myhre, G., et al. (2016). Recommendations for diagnosing effective radiative forcing from climate models for CMIP6. *Journal of Geophysical Research: Atmospheres*, *121*, 12,460–12,475. https://doi.org/10.1002/2016JD025320

Furtado, K., Field, P. R., Boutle, I. A., Morcrette, C. J., & Wilkinson, J. M. (2016). A physically based subgrid parameterization for the production and maintenance of mixed-phase clouds in a general circulation model. *Journal of the Atmospheric Sciences*, *73*(1), 279–291. https://doi.org/10.1175/JAS-D-15-0021.1

Gantt, B., Meskhidze, N., Facchini, M. C., Rinaldi, M., Ceburnis, D., & O'Dowd, C. D. (2011). Wind speed dependent size-resolved parameterization for the organic mass fraction of sea spray aerosol. *Atmospheric Chemistry and Physics*, *11*(16), 8777–8790. https://doi.org/10.5194/acp-11-8777-2011

Ghan, S., Wang, M., Zhang, S., Ferrachat, S., Gettelman, A., Griesfeller, J., et al. (2016). Challenges in constraining anthropogenic aerosol effects on cloud radiative forcing using present-day spatiotemporal variability. *Proceedings of the National Academy of Sciences*, *113*(21), 5804–5811. https://doi.org/10.1073/pnas.1514036113

Golaz, J.-C., Horowitz, L. W., & Levy, H. (2013). Cloud tuning in a coupled climate model: Impact on 20th century warming. *Geophysical Research Letters*, *40*, 2246–2251. https://doi.org/10.1002/grl.50232

Golaz, J.-C., Salzmann, M., Donner, L. J., Horowitz, L. W., Ming, Y., & Zhao, M. (2011). Sensitivity of the aerosol indirect effect to subgrid variability in the cloud parameterization of the GFDL atmosphere general circulation model AM3. *Journal of Climate*, *24*(13), 3145–3160. https://doi.org/10.1175/2010JCLI3945.1

Grant, A. L. M., & Lock, A. P. (2004). The turbulent kinetic energy budget for shallow cumulus convection. *Quarterly Journal of the Royal Meteorological Society*, *130*(597), 401–422. https://doi.org/10.1256/qj.03.50

Grosvenor, D. P., Sourdeval, O., Zuidema, P., Ackerman, A., Alexandrov, M. D., Bennartz, R., et al. (2018). Remote sensing of droplet number concentration in warm clouds: A review of the current state of knowledge and perspectives. *Reviews of Geophysics*, *56*, 409–453. https://doi.org/10.1029/2017RG000593

Grosvenor, D. P., & Wood, R. (2014). The effect of solar zenith angle on MODIS cloud optical and microphysical retrievals within marine liquid water clouds. *Atmospheric Chemistry and Physics*, *14*(14), 7291–7321. https://doi.org/10.5194/acp-14-7291-2014

Gryspeerdt, E., Quaas, J., & Bellouin, N. (2016). Constraining the aerosol influence on cloud fraction. *Journal of Geophysical Research: Atmospheres*, *121*, 3566–3583. https://doi.org/10.1002/2015JD023744

Gryspeerdt, E., Quaas, J., Ferrachat, S., Gettelman, A. W., Ghan, S., Lohmann, U., et al. (2017). Constraining the instantaneous aerosol influence on cloud albedo. *Proceedings of the National Academy of Sciences*, *114*(19), 4899–4904. https://doi.org/10.1073/pnas.1617765114

Halloran, P. R., Bell, T. G., & Totterdell, I. J. (2010). Can we trust empirical marine DMS parameterisations within projections of future climate? *Biogeosciences*, *7*(5), 1645–1656. https://doi.org/10.5194/bg-7-1645-2010

Hamilton, D. S., Lee, L. A., Pringle, K. J., Reddington, C. L., Spracklen, D. V., & Carslaw, K. S. (2014). Occurrence of pristine aerosol environments on a polluted planet. *Proceedings of the National Academy of Sciences*, *111*(52), 18,466–18,471. https://doi.org/10.1073/pnas.1415440111

Hartmann, D., Tank, A. K., Rusticucci, M., Alexander, L., Brönnimann, S., Charabi, Y., et al. (2013). Observations: Atmosphere and surface. In T. F. Stocker, et al. (Eds.), *Climate Change 2013—The Physical Science Basis. Contribution of Working Group I to the Fifth Assessment Report of the Intergovernmental Panel on Climate Change* (pp. 159–254). Cambridge, UK: Cambridge University Press.

Haywood, J. M., Jones, A., Dunstone, N., Milton, S., Vellinga, M., Bodas-Salcedo, A., et al. (2016). The impact of equilibrating hemispheric albedos on tropical performance in the HadGEM2-ES coupled climate model. *Geophysical Research Letters*, *43*, 395–403. https://doi.org/10.1002/2015GL066903

Holben, B. N., Tanre, D., Smirnov, A., Eck, T. F., Slutsker, I., Abuhassan, N., et al. (2001). An emerging ground-based aerosol climatology: Aerosol optical depth from AERONET. *Journal of Geophysical Research*, *106*, 12,067–12,097. https://doi.org/10.1029/2001JD900014

Hourdin, F., Mauritsen, T., Gettelman, A., Golaz, J.-C., Balaji, V., Duan, Q., et al. (2017). The art and science of climate model tuning. *Bulletin of the American Meteorological Society*, *98*(3), 589–602. https://doi.org/10.1175/BAMS-D-15-00135.1

Huneeus, N., Schulz, M., Balkanski, Y., Griesfeller, J., Prospero, J., Kinne, S., et al. (2011). Global dust model intercomparison in AeroCom phase I. *Atmospheric Chemistry and Physics*, *11*(15), 7781–7816. https://doi.org/10.5194/acp-11-7781-2011

Hyder, P., Edwards, J. M., Allan, R. P., Hewitt, H. T., Bracegirdle, T. J., Gregory, J. M., et al. (2018). Critical Southern Ocean climate model biases traced to atmospheric model cloud errors. *Nature Communications*, *9*, 3625. https://doi.org/10.1038/s41467-018-05634-2

Jones, A., Roberts, D. L., Woodage, M. J., & Johnson, C. E. (2001). Indirect sulphate forcing in a climate model with an interactive sulphur cycle. *Journal of Geophysical Research*, *106*, 20,293–20,310.

Kettle, A. J., Andreae, M. O., Amouroux, D., Andreae, T. W., Bates, T. S., Berresheim, H., et al. (1999). A global database of sea surface dimethylsulfide (DMS) measurements and a procedure to predict sea surface DMS as a function of latitude, longitude, and month. *Global Biogeochemical Cycles*, *13*(2), 399–444. https://doi.org/10.1029/1999GB900004

Khairoutdinov, M. F., & Kogan, Y. L. (2000). A new cloud physics parameterization in a large-eddy simulation model of marine stratocumulus. *Monthly Weather Review*, *128*, 229–243.

Kinne, S., Schulz, M., Textor, C., Guibert, S., Balkanski, Y., Bauer, S. E., et al. (2006). An AeroCom initial assessment—Optical properties in aerosol component modules of global models. *Atmospheric Chemistry and Physics*, *6*, 1815–1834. https://doi.org/10.5194/acp-6-1815-2006

Kok, J. F., Ward, D. S., Mahowald, N. M., & Evan, A. T. (2018). Global and regional importance of the direct dust-climate feedback. *Nature Communications*, *9*, 241. https://doi.org/10.1038/s41467-017-02620-y

Korhonen, H., Carslaw, K. S., Spracklen, D. V., Mann, G. W., & Woodhouse, M. T. (2008). Influence of oceanic dimethyl sulfide emissions on cloud condensation nuclei concentrations and seasonality over the remote Southern Hemisphere oceans: A global model study. *Journal of Geophysical Research*, *113*, D15204. https://doi.org/10.1029/2007JD009718

Kretzschmar, J., Salzmann, M., Mülmenstädt, J., Boucher, O., & Quaas, J. (2017). Comment on "rethinking the lower bound on aerosol radiative forcing". *Journal of Climate*, *30*(16), 6579–6584. https://doi.org/10.1175/JCLI-D-16-0668.1

Lamarque, J.-F., Bond, T. C., Eyring, V., Granier, C., Heil, A., Klimont, Z., et al. (2010). Historical (1850–2000) gridded anthropogenic and biomass burning emissions of reactive gases and aerosols: Methodology and application. *Atmospheric Chemistry and Physics*, *10*, 7017–7039. https://doi.org/10.5194/acp-10-7017-2010

Lana, A., Bell, T. G., Simò, R., Vallina, S. M., Ballabrera-Poy, J., Kettle, A. J., et al. (2011). An updated climatology of surface dimethlysulfide concentrations and emission fluxes in the global ocean. *Global Biogeochemical Cycles*, *25*, GB1004. https://doi.org/10.1029/2010GB003850

Lewis, E. R., & Schwartz, S. E. (Eds.) (2004). *Sea Salt Aerosol Production: Mechanisms, Methods, Measurements, and Models Edited by* Lewis, E. R., & Schwartz, S. E. (pp. 9–13). Washington, DC: American Geophysical Union.

Liu, Y., & Daum, P. H. (2002). Indirect warming effect from dispersion forcing. *Nature*, *419*, 580. https://doi.org/10.1038/419580a

Liu, Y., Daum, P. H., Guo, H., & Peng, Y. (2008). Dispersion bias, dispersion effect, and the aerosol–cloud conundrum. *Environmental Research Letters*, *3*(4), 045,021.

Loeb, N. G., Wielicki, B. A., Doelling, D. R., Smith, G. L., Keyes, D. F., Kato, S., et al. (2009). Toward optimal closure of the Earth's top-of-atmosphere radiation budget. *Journal of Climate*, *22*(3), 748–766. https://doi.org/10.1175/2008JCLI2637.1

Lohmann, U., & Feichter, J. (2005). Global indirect aerosol effects: A review. *Atmospheric Chemistry and Physics*, *5*, 715–737.

Malavelle, F. F., Haywood, J. M., Jones, A., Gettelman, A., Clarisse, L., Bauduin, S., et al. (2017). Strong constraints on aerosol-cloud interactions from volcanic eruptions. *Nature*, *546*, 485. https://doi.org/10.1038/nature22974

Mann, G., Carslaw, K., Reddington, C., Pringle, K., Schulz, M., Asmi, A., et al. (2014). Intercomparison and evaluation of global aerosol microphysical properties among AeroCom models of a range of complexity. *Atmospheric Chemistry and Physics*, *14*(9), 4679–4713.

Mann, G. W., Carslaw, K. S., Spracklen, D. V., Ridley, D. A., Manktelow, P. T., Chipperfield, M. P., et al. (2010). Description and evaluation of GLOMAP-mode: A modal global aerosol microphysics model for the UKCA composition-climate model. *Geoscientific Model Development*, *3*(2), 519–551. https://doi.org/10.5194/gmd-3-519-2010

Martin, G. M., Johnson, D. W., & Spice, A. (1994). The measurement and parameterization of effective radius of droplets in warm stratocumulus clouds. *Journal of the Atmospheric Sciences*, *51*, 1823–1842.

McCoy, D. T., Burrows, S. M., Wood, R., Grosvenor, D. P., Elliott, S. M., Ma, P.-L., et al. (2015). Natural aerosols explain seasonal and spatial patterns of Southern Ocean cloud albedo. *Science Advances*, *1*(6), e1500157. https://doi.org/10.1126/sciadv.1500157

Meskhidze, N., & Nenes, A. (2006). Phytoplankton and cloudiness in the Southern Ocean. *Science*, *314*, 1419–1423. https://doi.org/10.1126/science.1131779

Mollard, J. (2017). Improving the simulation of carbonaceous aerosol in HadGEM3-UKCA. http://centaur.reading.ac.uk/75678/1/18001810_Mollard_thesis.pdf, last access: 19th April 2018.

Myhre, G., Samset, B. H., Schulz, M., Balkanski, Y., Bauer, S., Berntsen, T. K., et al. (2013). Radiative forcing of the direct aerosol effect from AeroCom phase ii simulations. *Atmospheric Chemistry and Physics*, *13*(4), 1853–1877. https://doi.org/10.5194/acp-13-1853-2013

Myhre, G., Shindell, D., Bron, F.-M., Collins, W., Fuglestvedt, J., Huang, J., et al. (2013). Anthropogenic and natural radiative forcing. In T. F. Stocker, et al. (Eds.), *Climate Change 2013—The Physical Science Basis. Contribution of Working Group I to the Fifth Assessment Report of the Intergovernmental Panel on Climate Change* (pp. 571–658). Cambridge, UK: Cambridge University Press.

Nazarenko, L., Rind, D., Tsigaridis, K., Genio, A. D., Kelley, M., & Tausnev, N. (2017). Interactive nature of climate change and aerosol forcing. *Journal of Geophysical Research: Atmospheres*, *122*, 3457–3480. https://doi.org/10.1002/2016JD025809

O'Dowd, C. D., Facchini, M. C., Cavalli, F., Ceburnis, D., Mircea, M., Decesari, S., et al. (2004). Biogenically driven organic contribution to marine aerosol. *Nature*, *431*, 676–680. https://doi.org/10.1038/nature02959

Paynter, D., & Frölicher, T. L. (2015). Sensitivity of radiative forcing, ocean heat uptake, and climate feedback to changes in anthropogenic greenhouse gases and aerosols. *Journal of Geophysical Research: Atmospheres*, *120*, 9837–9854. https://doi.org/10.1002/2015JD023364

Peng, Y., & Lohmann, U. (2003). Sensitivity study of the spectral dispersion of the cloud droplet size distribution on the indirect aerosol effect. *Geophysical Research Letters*, *30*(10), 1507. https://doi.org/10.1029/2003GL017192

Pincus, R., Forster, P. M., & Stevens, B. (2016). The Radiative Forcing Model Intercomparison Project (RFMIP): Experimental protocol for CMIP6. *Geoscientific Model Development*, *9*(9), 3447–3460. https://doi.org/10.5194/gmd-9-3447-2016

Quaas, J., Ming, Y., Menon, S., Takemura, T., Wang, M., Penner, J. E., et al. (2009). Aerosol indirect effects—General circulation model intercomparison and evaluation with satellite data. *Atmospheric Chemistry and Physics*, *9*(22), 8697–8717. https://doi.org/10.5194/acp-9-8697-2009

Quinn, P. K., & Bates, T. S. (2011). The case against climate regulation via oceanic phytoplankton sulphur emissions. *Nature*, *480*, 51. https://doi.org/10.1038/nature10580

Regayre, L., Johnson, J., Yoshioka, M., Pringle, K., Sexton, D., Booth, B., et al. (2018). Aerosol and physical atmosphere model parameters are both important sources of uncertainty in aerosol ERF. *Atmospheric Chemistry and Physics Discussions*, *18*, 9975–10,006.

Ridley, J. K., Blockley, E. W., Keen, A. B., Rae, J. G. L., West, A. E., & Schroeder, D. (2018). The sea ice model component of HadGEM3-GC3.1. *Geoscientific Model Development*, *11*, 713–723. https://doi.org/10.5194/gmd-2017-212

Rinaldi, M., Fuzzi, S., Decesari, S., Marullo, S., Santoleri, R., Provenzale, A., et al. (2013). Is chlorophyll-a the best surrogate for organic matter enrichment in submicron primary marine aerosol? *Journal of Geophysical Research: Atmospheres*, *118*, 4964–4973. https://doi.org/10.1002/jgrd.50417

Rothenberg, D., Avramov, A., & Wang, C. (2017). On the representation of aerosol activation and its influence on model-derived estimates of the aerosol indirect effect. *Atmospheric Chemistry and Physics Discussions*, *18*, 7961–7983.

Rotstayn, L. D., Collier, M. A., Shindell, D. T., & Boucher, O. (2015). Why does aerosol forcing control historical global-mean surface temperature change in CMIP5 models? *Journal of Climate*, *28*(17), 6608–6625. https://doi.org/10.1175/JCLI-D-14-00712.1

Rotstayn, L. D., & Liu, Y. (2003). Sensitivity of the first indirect aerosol effect to an increase of cloud droplet spectral dispersion with droplet number concentration. *Journal of Climate*, *16*(21), 3476–3481.

Rotstayn, L. D., & Liu, Y. (2009). Cloud droplet spectral dispersion and the indirect aerosol effect: Comparison of two treatments in a GCM. *Geophysical Research Letters*, *36*, L10801. https://doi.org/10.1029/2009GL038216

Sayer, A., Munchak, L., Hsu, N. C., Levy, R. C., Bettenhausen, C., & Jeong, M.-J. (2014). MODIS Collection 6 aerosol products: Comparison between Aqua's e-Deep Blue, Dark Target, and merged data sets, and usage recommendations. *Journal of Geophysical Research: Atmospheres*, *119*, 13,965–13,989. https://doi.org/doi:10.1002/2014JD022453

Schmidt, G. A., Bader, D., Donner, L. J., Elsaesser, G. S., Golaz, J.-C., Hannay, C., et al. (2017). Practice and philosophy of climate model tuning across six US modeling centers. *Geoscientific Model Development*, *10*(9), 3207–3223. https://doi.org/10.5194/gmd-10-3207-2017

Schulz, M., Textor, C., Kinne, S., Balkanski, Y., Bauer, S., Berntsen, T., et al. (2006). Radiative forcing by aerosols as derived from the AeroCom present-day and pre-industrial simulations. *Atmospheric Chemistry and Physics*, *6*, 5225–5246. https://doi.org/10.5194/acp-6-5225-2006

Schwartz, S. E. (1998). Are the global cloud albedo and climate controlled by marine phytoplankton. *Nature*, *336*, 441–445. https://doi.org/10.1038/336441a0

Scott, C. E., Arnold, S. R., Monks, S. A., Asmi, A., Paasonen, P., & Spracklen, D. V. (2018). Substantial large-scale feedbacks between natural aerosols and climate. *Nature Geoscience*, *11*, 44–48. https://doi.org/10.1038/s41561-017-0020-5

Seinfeld, J. H., Bretherton, C., Carslaw, K. S., Coe, H., DeMott, P. J., Dunlea, E. J., et al. (2016). Improving our fundamental understanding of the role of aerosol-cloud interactions in the climate system. *Proceedings of the National Academy of Sciences*, *113*(21), 5781–5790. https://doi.org/10.1073/pnas.1514043113

Sherwood, S. C., Bony, S., Boucher, O., Bretherton, C., Forster, P. M., Gregory, J. M., & Stevens, B. (2015). Adjustments in the forcing-feedback framework for understanding climate change. *Bulletin of the American Meteorological Society*, *96*(2), 217–228. https://doi.org/10.1175/BAMS-D-13-00167.1

Shindell, D. T., Lamarque, J.-F., Schulz, M., Flanner, M., Jiao, C., Chin, M., et al. (2013). Radiative forcing in the ACCMIP historical and future climate simulations. *Atmospheric Chemistry and Physics*, *13*(6), 2939–2974. https://doi.org/10.5194/acp-13-2939-2013

Simò, R., & Dachs, J. (2002). Global ocean emission of dimethylsulfide predicted from biogeophysical data. *Global Biogeochemical Cycles*, *16*(4), 1018. https://doi.org/10.1029/2001GB001829

Spracklen, D. V., Arnold, S. R., Sciare, J., Carslaw, K. S., & Pio, C. (2008). Globally significant oceanic source of organic carbon aerosol. *Geophysical Research Letters*, *35*, l12811. https://doi.org/10.1029/2008GL033359

Stephens, G. L., Hakuba, M. Z., Hawcroft, M., Haywood, J. M., Behrangi, A., Kay, J. E., & Webster, P. J. (2016). The curious nature of the hemispheric symmetry of the Earth's water and energy balances. *Current Climate Change Reports*, *2*(4), 135–147. https://doi.org/10.1007/s40641-016-0043-9

Stevens, B. (2015). Rethinking the lower bound on aerosol radiative forcing. *Journal of Climate*, *28*(12), 4794–4819. https://doi.org/10.1175/JCLI-D-14-00656.1

Storelvmo, T., Lohmann, U., & Bennartz, R. (2009). What governs the spread in shortwave forcings in the transient IPCC AR4 models? *Geophysical Research Letters*, *36*, L01806. https://doi.org/10.1029/2008GL036069

Storkey, D., Blaker, A. T., Mathiot, P., Megann, A., Aksenov, Y., Blockley, E. W., et al. (2018). UK Global Ocean GO6 and GO7: A traceable hierarchy of model resolutions. *Geoscientific Model Development Discussions*, *2018*, 1–43. https://doi.org/10.5194/gmd-2017-263

Suzuki, K., Golaz, J.-C., & Stephens, G. L. (2017). Evaluating cloud tuning in a climate model with satellite observations. *Geophysical Research Letters*, *40*, 4464–4468. https://doi.org/10.1002/grl.50874

Textor, C., Schulz, M., Guibert, S., Kinne, S., Balkanski, Y., Bauer, S., et al. (2006). Analysis and quantification of the diversities of aerosol life cycles within AeroCom. *Atmospheric Chemistry and Physics*, *6*(7), 1777–1813. https://doi.org/10.5194/acp-6-1777-2006

Twomey, S. (1974). Pollution and the planetary albedo. *Atmospheric Environment*, *8*, 1251–1256.

Voigt, A., Stevens, B., Bader, J., & Mauritsen, T. (2013). The observed hemispheric symmetry in reflected shortwave irradiance. *Journal of Climate*, *26*(2), 468–477. https://doi.org/10.1175/JCLI-D-12-00132.1

World Climate Research Program (1986). A preliminary cloudless standard atmosphere for radiation computation (*Rep. WCP, 112, 53*). Geneva, Switzerland. World Meteorological Organization(WMO).

Walters, D., Baran, A., Boutle, I., Brooks, M., Earnshaw, P., Edwards, J., et al. (2017). The met office unified model global atmosphere 7.0/7.1 and JULES global land 7.0 configurations. *Geoscientific Model Development Discussions*, *2017*, 1–78. https://doi.org/10.5194/gmd-2017-291

West, R. E. L., Stier, P., Jones, A., Johnson, C. E., Mann, G. W., Bellouin, N., et al. (2014). The importance of vertical velocity variability for estimates of the indirect aerosol effects. *Atmospheric Chemistry and Physics*, *14*(12), 6369–6393. https://doi.org/10.5194/acp-14-6369-2014

Wilcox, L. J., Highwood, E. J., Booth, B. B. B., & Carslaw, K. S. (2015). Quantifying sources of inter-model diversity in the cloud albedo effect. *Geophysical Research Letters*, *42*, 1568–1575. https://doi.org/10.1002/2015GL063301

Woodhouse, M. T., Carslaw, K. S., Mann, G. W., Vallina, S. M., Vogt, M., Halloran, P. R., & Boucher, O. (2010). Low sensitivity of cloud condensation nuclei to changes in the sea-air flux of dimethyl-sulphide. *Atmospheric Chemistry and Physics*, *10*(16), 7545–7559. https://doi.org/10.5194/acp-10-7545-2010

Woodward, S. (2001). Modelling the atmospheric life cycle and radiative impact of mineral dust in the Hadley Centre climate model. *Journal of Geophysical Research*, *106*(D16), 18,155–18,166.

Xie, X., & Liu, X. (2013). Analytical studies of the cloud droplet spectral dispersion influence on the first indirect aerosol effect. *Advances in Atmospheric Sciences*, *30*(5), 1313–1319. https://doi.org/10.1007/s00376-012-2141-5

Zelinka, M. D., Andrews, T., Forster, P., & Taylor, K. E. (2014). Quantifying components of aerosol-cloud-radiation interactions in climate models. *Journal of Geophysical Research: Atmospheres*, *119*, 7599–7615. https://doi.org/10.1002/2014JD021710